



Evaluating the effects of columnar NO₂ on the accuracy of aerosol optical properties retrievals

Theano Drosoglou¹, Ioannis-Panagiotis Raptis^{1,2}, Massimo Valeri³, Stefano Casadio³, Francesca Barnaba⁴, Marcos Herreras-Giralda⁵, Anton Lopatin⁵, Oleg Dubovik⁶, Gabriele Brizzi⁷, Fabrizio Niro⁷,
5 Monica Campanelli⁴, Stelios Kazadzis⁸

¹Institute for Environmental Research and Sustainable Development, National Observatory of Athens (IERSD/NOA), 15236 Athens, Greece

²Laboratory of Climatology and Atmospheric Environment, Sector of Geography and Climatology, Department of Geology and Environment, National and Kapodistrian University of Athens, Athens, GR-15784, Greece

10 ³Serco Italia S.p.A., Frascati, Rome, Italy

⁴National Research Council, Institute of Atmospheric Sciences and Climate, CNR- ISAC, National Research Council, Rome, Italy

⁵GRASP SAS, Remote Sensing Developments, 59260 Lezennes, France

⁶Univ. Lille, CNRS, UMR 8518 - LOA - Laboratoire d'Optique Atmosphérique, Lille, France

15 ⁷ESA-ESRIN, Frascati, Rome, Italy

⁸Physicalisch-Meteorologisches Observatorium Davos, World Radiation Center, CH-7260 Davos, Switzerland

Correspondence to: Theano Drosoglou (tdroso@noa.gr)

Abstract. We aim to evaluate the NO₂ absorption effect in aerosol properties derived from sun-sky radiometers as well as the possible retrieval algorithm improvements by using more accurate characterization of NO₂ optical depth. For this purpose, we
20 employ multiannual (2017-2022) records of Aerosol Optical Depth (AOD), Ångström Exponent (AE) and Single Scattering Albedo (SSA) collected by sun photometers at an urban and a suburban site in the Rome area (Italy) in the framework of both the AERONET and SKYNET networks. The uncertainties introduced in the retrievals by the NO₂ absorption are investigated using high-frequency observations of total NO₂ derived from co-located Pandora spectroradiometer systems as well as space-
borne NO₂ products from the Tropospheric Monitoring Instrument (TROPOMI). The correction is useful for lower AODs (<
25 0.3), where the majority of observations is found, especially under high NO₂ pollution events. The analysis does not reveal any significant impact of the NO₂ correction on the derived aerosol temporal trends for the very limited data sets used in this study. However, the effect is expected to become more evident for trends derived from larger data sets as well as in the case of an important NO₂ trend. In addition, the comparisons of the NO₂-modified ground-based AOD data with satellite retrievals from the Deep Blue (DB) algorithm of the NASA Moderate Resolution Imaging Spectroradiometer (MODIS) resulted in a
30 slight improvement in the agreement of about 0.003 and 0.006 for AERONET and SKYNET, respectively. Finally, the uncertainty in assumptions of NO₂ seem to have a non-negligible impact on the retrieved values of SSA at 440 nm leading to an average positive bias of 0.02 (2.5 %) in both locations for high NO₂ loadings (> 0.9 DU).



1 Introduction

Atmospheric particles possess both direct and indirect effects on Earth's radiation budget and climate (IPCC, 2013). Direct radiative forcing arises from aerosols interaction with solar radiation through absorption and scattering processes (Hobbs, 1993). As an indirect impact, aerosols play an important role in cloud formation and properties by acting as cloud condensation nuclei on which water vapour condenses and by influencing the cloud albedo and lifetime (Rosenfeld et al., 2014). Moreover, heterogeneous chemical reactions can take place on the surfaces of atmospheric particles having a crucial effect on atmospheric chemistry and composition. Examples of such aerosol-driven reactions are those that lead to stratospheric ozone depletion in the polar regions (Solomon et al., 1986). In addition to their footprint on radiative forcing and climate, aerosols adversely affect human health and have been associated with a wide variety of health issues such as respiratory and neurological diseases, cancer, diabetes, cardiovascular diseases and hypertension (e.g., Lelieveld et al., 2015; Molina et al., 2020 and references therein).

The above effects of airborne particulate matter on Earth's climate and human health strongly depend on the intra-annual variations in its loading and properties. The most widely used variable for the estimation of columnar aerosol concentration in the atmosphere is the multi-wavelength Aerosol Optical Depth (AOD). Aerosol optical properties are monitored globally by satellite, e.g., the Moderate Resolution Imaging Spectroradiometer (MODIS) and ground-based networks of sun-photometers like Aerosol Robotic Network (AERONET) (Holben et al., 1998), SKYNET (Nakajima et al., 2020) or the Global Atmosphere Watch Precision Filter Radiometer (GAW-PFR) network (Kazadzis et al., 2018a). Ground-based remote sensing allows accurate AOD retrievals, i.e. in the order of 0.01 – 0.02 depending on the AOD wavelength (Kazadzis et al., 2018b), which are in fact widely used as a validation reference for satellite or model-based AOD products (e.g., Chu et al., 2002; Remer et al., 2005; Green et al., 2009; Levy et al., 2010; Li et al., 2015; Sherman et al., 2016; Gkikas et al., 2021; Di Tomaso et al., 2022) and used as inputs on various modelling initiatives (e.g., Benedetti et al., 2018).

However, AOD retrieval from sun-photometers includes some assumptions in order to take into account all the non-aerosol effects in the retrieval spectral range. In particular, AOD retrievals are sensitive to the assumptions on the concentration of atmospheric trace gases, absorbing in the instrument spectral bands considered, among which are ozone (O₃) and nitrogen dioxide (NO₂). The exact effect of trace gases in the retrieval at a particular bandwidth depends also on their absorption cross section. For the case of NO₂, as filter radiometers retrieve the AOD in certain wavelength bands based on their filter responsivity, such retrievals, especially in the standard wavelengths of 380 and 440 nm (AERONET), have to be corrected for the NO₂ optical depth. Currently, some AOD retrievals do not take NO₂, i.e. NO₂ optical depth, into consideration when deriving AOD (e.g., SKYNET, GAW-PFR) while others use satellite-based climatological NO₂ data sets for estimating it (e.g., AERONET). In the case of the GAW-PFR network, the error introduced in AOD retrievals by NO₂ absorption can be assumed to be negligible due to the low NO₂ concentrations observed in the GAW remote stations (the annual mean values of NO₂ optical depth are in general < 0.001) (Kazadzis et al., 2018a). However, especially over polluted areas, NO₂ is characterized by rather short lifetime and high spatiotemporal variations, due to inhomogeneous local emission patterns and photochemical



destruction (e.g., Richter et al., 2005; Boersma et al., 2008; Tzortziou et al., 2014, 2015; Drosoglou et al., 2017; Fan et al., 2021). Although the stratospheric component of NO₂ is quite stable spatially, the tropospheric NO₂ is highly variable in space and time and can bias the calculation of AOD if neglected (Arola and Koskela, 2004; Boersma et al., 2004). Hence, areas with high tropospheric NO₂ emission will tend to have greater proclivity for deviating from climatological mean values which might not be representative of the actual NO₂ loading and spatial distribution in the atmosphere, introducing potential errors in AOD calculations in those spectral regions with significant NO₂ absorption footprint.

Satellite observations with improved spatial and temporal resolution, e.g., the Sentinel-5Precursor Tropospheric Monitoring Instrument (S5P/TROPOMI), models, or co-location with surface-based Pandora instruments from Pandonia Global Network (PGN) spectroradiometers (Cede et al., 2020) measuring total column of NO₂ may assist in reducing the uncertainty of the NO₂ optical depth contribution in later versions of AOD retrieval algorithms. In the present study, we aim at evaluating if and how much AOD as well as its spectral variability, i.e., the associated Ångström Exponent (AE), and Single Scattering Albedo (SSA) retrievals could be improved by applying a specific correction using synchronous and co-located measurements of total NO₂ column from Pandonia network spectroradiometers. To this purpose, we exploit the unique configuration of twin observational sites in the Rome area (Italy), where multiannual (2017-2022) records of both multispectral AOD observations and columnar NO₂ measurements are available both in the city centre and in a suburban location. High-frequency measurements of total NO₂ performed by co-located Pandora spectroradiometer systems along with relatively high spatially resolved NO₂ observations from the S5P/TROPOMI satellite sensor were used to evaluate the current uncertainty in the retrievals of aerosol properties. Aerosol retrieval modifications based on Pandora NO₂ measurements are proposed for both AERONET and SKYNET. A first attempt to investigate the impact of those corrections on AOD and AE annual trends is also conducted.

2 Instrumentation, data and methodology

2.1 The target area and relevant observational sites

Rome is the capital and the most populous city of Italy with almost 3 million inhabitants and one of the most densely populated cities in the European Union (ISTAT 2021). It is located about 24 km east of the Tyrrhenian Sea, surrounded by an extensive undulating plain and crossed by Tiber and Aniene rivers. The city is part of the Lazio administrative region in the central part of the Italian peninsula. The economic activities in the metropolitan area are characterized by the absence of heavy industrial facilities and are related mainly to the services and high-technology sectors as well as commercial activities and tourism. The city air quality is strongly affected by local emission sources, such as transportation and domestic heating, but it is also markedly affected by local circulation and mid-to-long range transport events of sea salt, wildfires and Saharan dust (e.g., Ciardini et al., 2012; Gobbi et al. 2013; Valentini et al, 2020; Di Bernardino et al., 2021).

Rome air quality is monitored on a regular basis by standard in situ instrumentation. These measurements are complemented by multi-platform, long-term observations of aerosol and trace gases performed by a variety of ground-based remote sensing



instruments such as sun-sky radiometers, Raman and elastic lidars, automated lidar-ceilometers, Pandora, Brewer and DOAS spectrophotometers (e.g., Di Ianni et al., 2018; Iannarelli et al., 2021; Diemoz et al., 2021; Bellini et al., 2023). In this study, we used remote sensing measurements of columnar NO₂ and aerosol properties performed in two stations located in the greater area of Rome. More specifically observations were obtained from an urban station (APL-SAP hereafter) located at the Atmospheric Physics Laboratory of the Physics Department of ‘La Sapienza’ University in the city centre (41.90° N, 12.52° E; altitude 75 m a.s.l.) and a suburban site at the southern east edge of the city in the CNR-ISAC Rome Atmospheric Supersite, CIRAS, in Rome-Tor Vergata (41.84° N, 12.65° E; altitude 117 m a.s.l.). These two observational sites along with the rural station of CNR-IIA in Montelibretti contribute to the Boundary-layer Air Quality-analysis Using Network of Instruments (BAQUNIN) supersite (Iannarelli et al., 2021).

2.2 Aerosol data sets

2.2.1 AERONET

The Aerosol Robotic Network (AERONET) is a ground-based passive remote sensing aerosol monitoring network initiated by NASA and expanded by several national and international networks and collaborators (Holben et al., 1998). For more than two decades, AERONET has been delivering continuous, long-term data sets of aerosol optical, microphysical and radiative properties to support aerosol studies and validation of space-borne retrievals. The network uses the Cimel CE318-T Sun-Sky-Lunar multispectral photometers and provides standardization of instrument calibration and data acquisition as well as centralized data processing and distribution. The AERONET public domain database provides retrievals of spectral AOD, inversion products and precipitable water at a global scale (<https://aeronet.gsfc.nasa.gov/>, last access: 21 October 2022).

In this study, we employed Level 1.5 quality-assured retrievals of AOD at 380, 440, 500, 675 and 870 nm along with AE at 440-870 nm from Version 3 processing algorithm (Giles et al., 2019; Sinyuk et al., 2020). Level 1.5 data are cloud-screened and quality-assured, but final calibration may not have been applied to them. However, they represent a good trade-off between quality and readiness, considering that our approach aims to perform a near-real-time improvement on aerosol products. For AOD retrieval, the NO₂ optical depth is estimated from monthly climatological values of total NO₂ from OMI/Aura Level-3 retrievals during the 2004-2013 period at 0.25° by 0.25° spatial resolution and the NO₂ absorption coefficients from Burrows et al. (1998). The observations over the CNR-ISAC station used in this work cover the period March 2017 – mid-August 2022 (Fig. 1), in which synchronous data from the co-located Pandora instrument are available. The respective period for APL-SAP is from April 2017 through early September 2022 (Fig. 1).

In addition, we employed Level 1.5 SSA retrievals at 440 nm from almucantar measurements performed at both AERONET stations. Almucantar scans (circle on the celestial sphere parallel to the horizon) are measurements of radiance as a function of scattering angle performed by CIMEL instruments in order to be used for the retrieval of inversion products such as optical absorption (SSA), aerosol scattering phase function and properties related to aerosol typing, e.g., aerosol volume size distribution and complex refractive index (Dubovik and King, 2000; Dubovik et al., 2000). SSA is a measure of the



130 scattering/absorbing nature of aerosol mixture and theoretically ranges between 0 and 1. In Earth's atmosphere, its value is usually very close to 1, as most aerosols types mainly scatter solar light, and it is rarely found lower than 0.7 (Dubovik et al., 2002; Raptis et al., 2020). The complete SSA data set used for this study is formed by 1478 retrievals spanning from March 2017 to November 2020 in the case of APL-SAP station, and 2463 spanning from April 2017 to September 2021 for CNR-ISAC.

135 2.2.2 SKYNET

The SKYNET network, established at the beginning of 2000s, is a ground-based radiation observation network dedicated to aerosol, cloud and solar radiation interaction researches using the Prede POM sun-sky radiometers (Takamura and Nakajima, 2004; Nakajima et al., 2020). It is based on the collaboration and maintenance by several universities and research institutes around the world. This network imposes the standardization of instrument calibration, data acquisition and data processing and implements two data analysis flows (SR-CEReS & ESR-MRI) mainly based on the SKYRAD.pack, a software package implemented for the POM sky radiometer (e.g., Nakajima et al., 1996) (<https://www.skynet-isdc.org/methodology.php>, last access: 21 October 2022). In contrast to AERONET AOD retrieval methodologies, no correction for NO₂ optical depth is applied in the calculation of SKYNET AOD (e.g., Campanelli et al., 2004; Estellés et al., 2012). Here, we used the ESR-MRI/SUNRAD processor version 0.9 Level 2 AOD at 400, 500, 675, 870, and 1020 nm and AE at 400-1020 nm data sets over APL-SAP from late September 2017 to May 2022 (Fig. 1), which are open-accessed online (<https://www.skynet-isdc.org/data.php>, last access: 21 October 2022).

2.2.3 MODIS Deep Blue data

The Moderate Resolution Imaging Spectroradiometer (MODIS) is a key sensor onboard the NASA Terra and Aqua satellites flying respectively since 2000 and 2002. Terra MODIS (descending node, about 10:30 a.m. UTC) and Aqua MODIS (ascending node, about 1:30 p.m. UTC) are observing the entire Earth's surface every 1 to 2 days, acquiring data in 36 spectral bands ranging in wavelength from 0.4 μm to 14.4 μm, with a spatial resolution of 1 km at nadir (except for a few bands with higher spatial resolution).

Inversion of MODIS observations allows retrievals of several geophysical quantities. Here, we used the aerosol AOD products retrieved using the MODIS Deep Blue (DB) algorithm (Hsu et al., 2004, 2006, 2013). The basic principle of DB algorithms is to utilize the pre-calculated land surface reflectance database in deep blue bands (0.412 μm), in which surface reflectance is relatively lower than those in longer bands. In particular, we used the Collection 6.1 DB AOD products for both Aqua and Terra satellites. More details about the DB algorithm are in Hsu et al. (2013) and references therein. The spatial resolution of this product is 10 km. Wei et al. (2019) highlighted that the DB algorithm is relatively more stable and less affected by changes in atmospheric and surface conditions with respect to the Dark Target algorithm (Levy et al., 2013), showing better performances in urban areas for slightly polluted cases, such as the area of Rome. They also highlighted that Collection 6.1 AOD products perform better than the previous collections, especially in Europe and North America. The MODIS DB products



used in this study are available at the Level-1 and Atmosphere Archive and Distribution System Distributed Active Archive Center (<http://ladsweb.nascom.nasa.gov>, last access: 21 October 2022).

2.3 Total NO₂ observations

165 2.3.1 Pandora spectroradiometers

Pandora instruments are compact spectrometers that perform spectral measurements with high temporal resolution of direct solar irradiance and scattered radiance for the retrieval of total and tropospheric column densities of atmospheric trace gases (e.g., NO₂, O₃ and HCHO) that affect air quality, as well as their near-surface concentrations and vertical profiles (e.g., Herman et al., 2009; Tzortziou et al., 2012, 2015). The total NO₂ data sets used in the present study were obtained from the Pandora spectrometer #115 operating at CNR-ISAC since March 2017 and the Pandora systems #117 and #138 both deployed at APL-SAP since April 2016 and within the period August 2019 – October 2020, respectively. The above time series have been affected by the COVID-19 lockdown period February – May 2020 (Campanelli et al., 2021). The monthly averaged values from both stations are presented in Fig. 2 and inter-compared in the scatterplot of Fig. 3. On average, the Pandora total NO₂ column over APL-SAP is about 0.07% higher compared to the CNR-ISAC NO₂.

175 Pandora total NO₂ column product is derived from the direct-sun measurements in the UV-VIS spectral range 280-530 nm with an average resolution of 0.6 nm by means of the Blick software and the algorithm implemented there as described by Cede (2021). The data sets employed for this work were obtained with the direct-sun retrieval code “nvs3” and the Blick processor version 1.8. Pandora instruments are part of the Pandonia Global Network (PGN) (Cede et al., 2020) and have been fully characterized following the calibration procedures presented by Müller et al. (2020). The recorded raw spectrally resolved radiation measurements are centrally processed for the retrieval of atmospheric trace gas products which are all publicly available online (<https://www.pandonia-global-network.org/>, last access: 21 October 2022). Pandora NO₂ retrievals have been compared and validated with other ground-based and space-borne observations during several field campaigns (e.g., Flynn et al., 2014; Martins et al., 2016; Lamsal et al., 2017; Herman et al., 2018; Kreher et al., 2020). Total NO₂ data from the Pandora instrument #117 located at APL-SAP have been compared with NO₂ observations retrieved by the co-located MkIV Brewer spectrophotometer with serial number #067 (Diémoz et al., 2021). In the current study, high (flags 0 and 10) and medium (flags 1 and 11) quality data are employed.

As already mentioned in Sect. 2.2.1, AERONET uses climatological values from OMI L3 products for the estimation of NO₂ optical depth in AOD retrievals. The corresponding OMI total NO₂ range between about 0.2 and 0.3 DU, with an average value of 0.26 (\pm 0.02) DU. The bivariate relative distribution of the percentage deviation of Pandora columnar NO₂ from the AERONET climatological values against the PGN product for both urban (APL-SAP) and suburban (CNR-ISAC) locations is illustrated in Fig. 4. The Pandora data are time-interpolated to AERONET measurements. The percentage frequency distributions of absolute Pandora-OMI deviation for both locations is also presented. A systematic OMI climatology underestimation (positive deviations) is observed for about 89% and 87% of the data pairs for APL-SAP and CNR-ISAC,



195 respectively (lower panel of Fig. 4). AERONET aerosol retrievals seem to significantly underestimate the NO₂ abundance over
urban and suburban locations with an average absolute difference between the actual Pandora measurements and the
estimations from satellite climatology of about 0.15 ± 0.19 DU ($61.5 \pm 71.5\%$) and 0.16 ± 0.18 DU ($61.5 \pm 67.2\%$) for APL-
SAP and CNR-ISAC, respectively. As expected, since OMI climatology cannot capture the temporal NO₂ variability, both the
absolute (not shown here) and percentage (Fig. 4) derived differences of total NO₂ are highly correlated to the Pandora
measurements. Most of the data pairs lie within 0-200 % deviation of PGN data from AERONET climatology corresponding
200 to Pandora values lower than 1 DU. More specifically, the 90% of PGN NO₂ data over APL-SAP differ within -0.14 DU (-
50%) and 0.44 DU (150%) from OMI climatology, while the respective deviation range between -0.14 and 0.51 DU (-50% –
170%) for CNR-ISAC. However, there are quite a few cases (~9.5% and ~8.8% for APL-SAP and CNR-ISAC, respectively)
of higher PGN values (< 2 DU) leading to larger deviations (up to 600%, i.e. ~1.6 DU for APL-SAP and ~1.5 DU for CNR-
ISAC).

205 2.3.2 TROPOMI

The Tropospheric Monitoring Instrument (TROPOMI) is a nadir-viewing spectrometer on board Sentinel-5 Precursor (S5P)
satellite, launched on 13 October 2017. NO₂ columns are retrieved using the backscatter solar radiation detected in the spectral
window of 405-465 nm (van Geffen et al., 2015) by applying the DOAS technique (Platt, 1994; Platt and Stutz, 2008). The
operational TROPOMI NO₂ products are generated using the algorithm described by van Geffen et al. (2022), which is an
210 improvement of the NO₂ DOMINO algorithm (Boersma et al., 2011) developed by KNMI for the OMI satellite sensor
measurements. Both near-real-time (NRTI) and off-line (OFFL) NO₂ data sets are retrieved using the KNMI standard algorithm
(Eskes et al., 2022; Eskes and Eichmann, 2022). NRTI data files are available within 3 hours from the measurement, whereas
the OFFL data are processed in off-line mode and the respective files are generated a few days after the sensing time (van
Geffen et al., 2022).

215 In this study, the OFFL NO₂ retrievals are employed, which are the main S5P/TROPOMI product. The extracted NO₂ data set
covers the period October 2018 – August 2022 and includes observations obtained from several processor versions; beginning
with version 01.02.00 before March 2019 and going up to version 02.04.00 after July 2022. The total NO₂ column was
calculated from the sum of the tropospheric and stratospheric components, which is preferred over the TROPOMI total NO₂
product for comparisons with ground-based data, because the latter suffers from retrieval uncertainties due to its significant
220 dependence on the ratio of the a-priori tropospheric and stratospheric columnar data (van Geffen et al., 2022). Additionally,
the satellite pixels have been filtered to keep only those with QA value > 0.75, corresponding to cloud radiance fractions < 0.5
(Eskes and Eichmann, 2022). The S5P/TROPOMI NO₂ products have been downloaded from the Sentinel-5P Pre-Operations
Data Hub of the Copernicus Open Access Hub (<https://scihub.copernicus.eu/>, last access: 21 October 2022).

For visualization purposes, averages of the summed NO₂ column re-gridded on a 500m grid are plotted for the greater Rome
225 area (Fig. 5). The data used in Fig. 5 cover the period from 2018 to 2021, excluding the COVID-19 lockdown period (February
– May 2020).



2.4 Methodology

2.4.1 AOD retrievals

The methodology to derive AOD (also referred to as τ) from photometric measurements is based on the Lambert-Beer law (Eq. 1), which describes light attenuation by atmospheric components. $I_0(\lambda)$ is the intensity of the incident light and $I(\lambda)$ denotes the radiation intensity after traversing through the atmosphere at a specific wavelength λ .

$$I(\lambda) = I_0(\lambda) \cdot e^{-(m_\tau(\lambda)\tau(\lambda) + m_R(\lambda)\tau_R(\lambda) + \sum_j m_j(\lambda)\tau_j(\lambda))}, \quad (1)$$

$$\frac{\ln I(\lambda)}{\ln I_0(\lambda)} = -(m_\tau(\lambda)\tau(\lambda) + m_R(\lambda)\tau_R(\lambda) + \sum_j m_j(\lambda)\tau_j(\lambda)), \quad (2)$$

The quantities τ and τ_R describe the optical depth of radiation extinction due to aerosols (Mie scattering) and atmospheric molecules (Rayleigh scattering), whereas m_τ and m_R are the respective air mass factors. $\sum_j m_j\tau_j$ represents the sum of the extinction due to absorption from atmospheric gases (Eq. 3), this depending on wavelength.

$$\sum_j m_j(\lambda)\tau_j(\lambda) = m_{NO_2}(\lambda)\tau_{NO_2}(\lambda) + m_{O_3}(\lambda)\tau_{O_3}(\lambda) + m_{H_2O}(\lambda)\tau_{H_2O}(\lambda) + \dots, \quad (3)$$

In our study we investigate the effects of using an independent, direct measurement of $\tau_{NO_2}(\lambda)$ rather than the climatological value used in the AERONET inversion in determining the AOD (τ). Thus, by combining Eq. (2) with Eq. (3), assuming that the air mass factor in direct-sun measurements is equal to $\sec(\theta)$ for both aerosol and NO_2 , where θ is the solar zenith angle, and absorption from all the other gaseous components keeps the same, the difference in AOD due to the different estimation of NO_2 optical depth is obtained by Eq. (4):

$$\Delta\tau(\lambda) = \tau_{NO_2PGN}(\lambda) - \tau_{NO_2AER}(\lambda), \quad (4)$$

where τ_{NO_2AER} is the NO_2 absorption optical depth climatology used by AERONET and τ_{NO_2PGN} is the optical depth calculated from Pandora NO_2 measurements. The latter is derived using Eq. (5):

$$\tau_{NO_2PGN}(\lambda) = \sigma_{NO_2}(\lambda) \cdot c_{NO_2PGN}, \quad (5)$$

The quantity $\sigma_{NO_2}(\lambda)$ in Eq. (5) refers to the absorption cross section of NO_2 at wavelength λ (Burrows et al., 1998) and c_{NO_2PGN} is the total NO_2 column from Pandora instrument. The modified AOD values (τ_{AER_mod}) are obtained from the standard AERONET AOD (τ_{AER}) by applying the following equation:

$$\tau_{AER_mod}(\lambda) = \tau_{AER}(\lambda) - \left((\sigma_{NO_2}(\lambda) \cdot c_{NO_2PGN}) - \tau_{NO_2AER}(\lambda) \right), \quad (6)$$

The same approach was also applied to the SKYNET AOD data. However, since the SKYNET retrievals assume $\tau_{NO_2SKYNET} = 0$, Eq. (4) and (6) are modified as:

$$\Delta\tau(\lambda) = \sigma_{NO_2}(\lambda) \cdot c_{NO_2PGN}, \quad (7)$$



$$\tau_{SKYNET_mod}(\lambda) = \tau_{SKYNET}(\lambda) - (\sigma_{NO_2}(\lambda) \cdot c_{NO_2PGN}), \quad (8)$$

255 where $\tau_{SKYNET}(\lambda)$ denotes the standard SKYNET AOD at spectral channel λ and $\tau_{SKYNET_mod}(\lambda)$ is the modified AOD at wavelength λ .

2.4.2 AE retrievals

The spectral variability of AOD is generally expressed as:

$$\tau = \beta \cdot \lambda^{-\alpha}, \quad (9)$$

$$260 \quad \ln \tau = \ln \beta - \alpha \cdot \ln \lambda, \quad (10)$$

where α stands for the Ångström Exponent (AE).

In AERONET (Eck et al., 1999), AE is calculated by applying a least squares regression fit on Eq. (10) using the AOD and wavelength logarithms for each non-polarized wavelength channels in different spectral ranges, i.e. 340-440, 380-500, 440-675, 440-870 and 500-870 nm. The negative slope of this linear fit is the Ångström exponent α (Eq. 11).

$$265 \quad \alpha = - \frac{N \sum \ln \tau_i \ln \lambda_i - \sum \ln \lambda_i \sum \ln \tau_i}{N \sum (\ln \lambda_i)^2 - (\sum \ln \lambda_i)^2}, \quad (11)$$

Here, we also investigate the impact of using synchronous Pandora total NO₂ data in AOD algorithm as described in Sect. 2.4.1 on AE retrievals. For this, the AERONET AE product in the range 440-870 nm was used along with the AOD of non-polarized channels included in this range, i.e., 440, 500, 675 and 870 nm. AE was recalculated based on Eq. (11) using the modified AOD at wavelengths 440 and 500 nm obtained from Eq. (6). For the other channels (675 and 870 nm), in which NO₂ absorption is negligible, the standard AOD data from AERONET were employed.

270 For SKYNET, AE is calculated by applying a least squares regression fit on Eq. (10) using the AOD and wavelength logarithms at all wavelengths 400, 500, 675, 870, and 1020 nm. Again, AOD was recalculated using Eq. (8) only at wavelengths 400 and 500 nm, where the impact of NO₂ absorption is significant.

The difference in AE due to the different estimation of NO₂ optical depth in AOD retrievals is expressed as:

$$275 \quad \Delta\alpha(\lambda) = \alpha_{mod}(\lambda) - \alpha(\lambda), \quad (12)$$

where $\alpha_{mod}(\lambda)$ represents the modified AE data and $\alpha(\lambda)$ denotes the AE standard product from AERONET or SKYNET network.

2.4.3 Trend calculations

280 In this study we also evaluate the impact of AOD and AE modified retrievals, as described in Sect. 2.4.1 and 2.4.2, on aerosol temporal trends. This is only a first attempt to investigate the possible effect on the AOD and AE trends since the data sets used here are quite short for statistically meaningful calculations.



The annual trends in AOD and AE were estimated by applying the weighted least squares fitting technique introduced by Weatherhead et al. (1998), previously adopted in several aerosol trend analysis studies from space and the ground (e.g., Zhang and Reid, 2010; Yoon et al., 2012; Logothetis et al., 2021). The applied linear trend model is based on the following formula:

$$285 \quad Y_t = \mu + \omega X_t + \varepsilon_t, \quad t = 1, \dots, T, \quad (13)$$

where Y_t is the monthly average aerosol property of interest, μ is a constant term representing the linear fit offset at the start of the time series, ω stands for the magnitude of the trend per year and ε_t is the monthly average noise not represented by the linear fit. $X_t = t/12$ is the decimal number of years since the first month of the time series, t is the month index, T denotes the total number of months and $T/12$ is the total number of years in the time series.

290 In order to account for data variability due to severe aerosol events and cloud disturbance, we introduced a monthly weighting factor w_t in the linear fitting procedure (Eq. 14) (Yoon et al., 2012). This weighting factor is defined as the square root of the number of observations available each month n_t divided by the monthly standard deviation σ_t (Eq. 15).

$$\chi^2(\mu, \omega) = \sum_{t=1}^T (w_t \cdot (Y_t - \mu - \omega X_t))^2, \quad (14)$$

$$w_t = \frac{\sqrt{n_t}}{\sigma_t}, \quad (15)$$

295 In order to derive statistically significant monthly mean values, a minimum number of 10 observations in a daily basis was ensured. In addition, qualified monthly averages require the availability of measurements from at least 10 days per month. Data were filtered based on the above criteria and days and/or months that did not fulfil them were excluded from the data sample used in the trend calculations. It should be noted that the data sets employed in this study are quite short for statistically meaningful aerosol trend analysis. However, this is a first attempt to investigate the impact of AOD and AE modified
300 calculations on the derived temporal trends.

3 Results and discussion

3.1 Differences in AOD and AE retrievals using Pandora NO₂ data

The differences in AOD ($\Delta\tau$) at 440 nm and, thus, of its spectral variability through the AE ($\Delta\alpha$ at 440-870 nm) correcting for measured NO₂ effects with respect to the standard AERONET retrievals are illustrated in Fig. 6 for both the Rome CNR-ISAC
305 and APL-SAP stations. $\Delta\tau$ is defined as the standard minus the modified AOD ($\tau_{\text{AER}} - \tau_{\text{AER_mod}}$, see Eq. 4-6), whereas $\Delta\alpha$ is defined as $\alpha_{\text{AER_mod}} - \alpha_{\text{AER}}$ (Eq. 12). The derived values are presented versus the AOD at 440 nm and are color-coded with respect to the Pandora NO₂ retrievals. The dependency of $\Delta\tau$ on NO₂ is quite clear. As expected, higher $\Delta\tau$ absolute values are obtained for higher NO₂ concentrations, regardless of the initial measured AOD. Also, the absolute percentage of $\Delta\tau$ with respect to the AOD is higher for lower aerosol loadings, which means that the impact of the NO₂ correction is more significant
310 on lower AODs. This fact is also clear from $\Delta\alpha$, which is higher not only for higher NO₂, but for lower AOD values as well.



Interestingly, the highest Pandora NO₂ retrievals are not associated to the highest AOD values, indicating that in Rome the high AOD loadings are not strictly associated to pollution events. Hence, it might be worth to modify aerosol retrievals for high NO₂ in those low and middle AOD pollution-related events.

315 In general, considering the climatological value chosen for Rome in AERONET retrievals, the use of actual, coincident NO₂ measurements on the calculations of aerosol properties seems to be still useful for AOD < 0.3, while quite negligible (less than 10%) for AOD > 0.5 and almost negligible for AOD > 0.8. In most cases AERONET retrievals seem to overestimate AOD and AE. However, there are cases of underestimation, especially in AE retrievals, which seems to be higher for lower AODs. Those underestimations correspond to overestimation of NO₂ from satellite monthly climatological values used in AERONET retrievals.

320 The results for SKYNET observations are similar (Fig. 7), but only positive $\Delta\tau$ and $\Delta\alpha$ values are derived, indicating overestimation of the aerosol properties, since the NO₂ optical depth is not considered in the standard retrieval processes (see Eq. 7-8). $\Delta\tau$ is defined as $\tau_{\text{SKYNET}} - \tau_{\text{SKYNET_mod}}$ (see Eq. 7-8), whereas $\Delta\alpha$ stands for $\alpha_{\text{SKYNET_mod}} - \alpha_{\text{SKYNET}}$ (Eq. 12). In addition, the derived deviations in aerosol properties reach higher values compared to AERONET. Especially AE differences extend up to a value of about 0.7, which is more than double compared to AERONET results. Interestingly, these quite large $\Delta\alpha$ values
325 (> 0.3) correspond to relatively low NO₂ loadings (< 1.2 DU). The differences observed between the two networks can be partly attributed to the different wavelength channels used for AOD and AE retrievals.

The statistics showing mean differences in AOD and AE AERONET and SKYNET retrievals using actual, coincident NO₂ measurements are presented in Table 1. AERONET AOD retrievals at 380 nm are also included in the table. In addition, deviations of AOD and AE using daily or monthly averages of NO₂ in AERONET and SKYNET observations are also
330 investigated. Table 1 shows that the average deviations of AOD and AE values do not change significantly whether the actual Pandora NO₂ measurements or the daily or monthly mean values are used for the retrievals. The percentage differences for AOD lie within the range 1.1 – 1.9% for AERONET while they are more than doubled (~ 5.5%) for SKYNET. For the standard aerosol products of the latter, NO₂ optical depth is not considered. The estimated percentage differences for AE are < 2% and > 2.5% for AERONET CNR-ISAC and APL-SAP, respectively, and about 7-8% for SKYNET APL-SAP. It should be noted
335 that the spectral channels used in AERONET retrievals are 380 and 440 nm for AOD and 440-870 nm for AE, whereas SKYNET data refer to 400 nm and 400-1020 nm for AOD and AE, respectively.

3.2 AOD and AE retrievals based on TROPOMI NO₂ data

Co-located S5P/TROPOMI observations, characterized by improved spatial and temporal resolution compared to previous satellite missions (e.g., OMI), were also employed to investigate whether the ground-based retrievals of aerosol properties
340 could be improved. Again, the approach described in Sect. 2.4.1 and 2.4.2 was applied by replacing the Pandora total NO₂ ($C_{\text{NO}_2\text{PGN}}$) with corresponding columnar retrievals from TROPOMI.

The statistical metrics of the averaged deviations of the modified AERONET and SKYNET AOD and AE retrievals using actual, co-located TROPOMI NO₂ measurements from the network standard products are presented in Table 2. Similarly to



Sect. 3.1 and Table 1, deviations of AOD and AE retrievals derived by employing daily or monthly mean TROPOMI total
345 NO₂ were also investigated. The average deviations of AOD and AE values do not change significantly whether the actual
TROPOMI NO₂ measurements or the daily mean values are used for the retrievals. This behaviour is expected considering
that TROPOMI overpasses occur once or twice per day, hence, they do not capture daily variations of NO₂. In the case of
monthly averaged TROPOMI NO₂ data, the estimated differences between the standard and modified aerosol products drop
notably for AERONET. However, there are still differences compared to OMI NO₂ climatology due to the improved spatial
350 resolution of TROPOMI pixel. Interestingly, the deviations of SKYNET retrievals using monthly TROPOMI data are very
similar to those derived using the actual overpasses or daily averaged TROPOMI NO₂, probably due to the fact that the NO₂
optical depth is not included in the standard network AOD retrieval processes.

The percentage differences for AOD lie within the range 0.1 – 0.9% for AERONET and are about 3.8% for SKYNET, which
are much lower compared to those derived using Pandora NO₂ (see Table 1). The estimated percentage differences for AE are
355 ~0.8% and ~1.6% for AERONET CNR-ISAC and APL-SAP, respectively, and about 4% for SKYNET APL-SAP using actual
or daily TROPOMI data. It should be noted again that the spectral channels used in AERONET retrievals are 380 and 440 nm
for AOD and 440-870 nm for AE, whereas SKYNET data refer to 400 nm and 400-1020 nm for AOD and AE, respectively.

3.3 Case study: Impact of high Pandora NO₂ on low AOD

In order to investigate further the impact of high NO₂ during pollution events on the retrieval of relatively low levels of AOD,
360 we used measurements performed at APL-SAP on June 25th 2020, in the morning of which there was a high NO₂ event. In the
upper panel of Fig. 8 and Fig. 9, the total NO₂ measured from Pandora during that day is illustrated. For AERONET (Fig. 8),
the satellite climatological values used in the retrieval of standard AOD product and their deviations from Pandora NO₂ are
also displayed. The standard and modified AOD and AE data from both AERONET and SKYNET, as well as the magnitude
of the respective differences ($\Delta\tau$ and $\Delta\alpha$), are presented in the middle and lower panels of both figures.

365 The differences in AOD and AE retrievals from both networks are significant only within a time span of about 3 hours around
the high NO₂ event (~7:00-10:00 UT) and can be assumed negligible for the rest of the day when the NO₂ levels remain quite
low. It can be also noted that in the case of SKYNET both AOD and AE deviations are a bit higher compared to the respective
AERONET deviations of synchronous data. This can be mainly attributed to the fact that SKYNET standard AOD retrieval
processes do not account for the NO₂ absorption and partly explained by the different channels used in the detectors of the two
370 networks.

3.4 Impact on AOD and AE trends

In this section, a first attempt is conducted to investigate the effect of the modified AOD and AE retrievals based on the
Pandora total NO₂ observations on the annual trends of those aerosol properties. The annual trends of AERONET/SKYNET
AOD and AE over both APL-SAP and CNR-ISAC sites, calculated by applying the approach described in paragraph 2.4.3, as
375 well as their uncertainties (standard errors of the regression slope) are presented in Table 3. In general, the calculated trends



from AERONET over the suburban area (CNR-ISAC) are quite higher compared to the AERONET-derived trends for the urban location (APL-SAP), but comparable with those from SKYNET. It should be noted here that the aerosol data sets from the two networks correspond to slightly different time periods. In addition, there are significant gaps in the time series from CNR-ISAC due to instrumental problems. The COVID-19 lockdown period (February – May 2020) has been excluded from
380 the data sets.

The results do not reveal any notable impact of NO₂-modified retrievals on AOD trends. It should be noted that the aerosol time series employed in this study are quite short (~5.5 years) for statistically meaningful trend analysis. In addition, the estimated trends are quite small and the uncertainties introduced by linear fit are relatively high, especially for AOD. Thus, we have not conducted any study on the significance of these trends. However, the NO₂ effect on the aerosol retrievals, although
385 small, is comparable with the calculated trends and may be significant for trends estimated over larger data sets. In addition, NO₂ effects on AOD trends would be more obvious in the case of a significant NO₂ trend during the period. AE trends with and without NO₂ correction show relatively higher differences as AE is much more sensitive to spectral AOD changes. However, the linear fitting uncertainty on AE is also high.

3.5 Inter-comparison of AERONET and SKYNET AOD products against MODIS DB AOD data

In this section, in addition to the analysis of ground-based data, we have analysed a potential effect of considered NO₂ corrections on the agreement of AERONET and SKYNET AOD products with satellite data. Indeed, it is well known that most satellite retrievals are validated against ground-based measurements of AOD that are considered as a ground-truth. Moreover, most satellite retrieval algorithms are substantially tuned to closely match AERONET observations. For example, all MODIS algorithms, including DB, rely, in one way or another, on AERONET dynamic aerosol models and climatologies
395 of AERONET retrievals. Nonetheless, since MODIS retrievals fundamentally rely on MODIS radiances that are fully independent of AERONET data, some inaccuracies in assumptions, such as those on NO₂ amount, can cause some additional biases between AERONET and MODIS AOD results.

To evaluate the effects of the proposed correction, we have compared AERONET and SKYNET AOD products against MODIS DB AOD products at 470 nm for the 2017-2022 period. In the inter-comparison, we considered only MODIS DB
400 AOD products for which the distance between the center of the pixel and the AERONET site location (APL-SAP or CNR-ISAC) does not exceed 5 km. Furthermore, we considered all the AERONET (or SKYNET) AOD data within ± 30 minutes from the MODIS satellite overpasses. In order to guarantee the quality of the data, we used MODIS DB AOD with QA index ≥ 2, which corresponds to good and very good products (Wei et al., 2019).

The inter-comparison has been performed using MODIS DB AOD at 470 nm. Consequently, we computed the AERONET
405 and SKYNET AOD at 470 nm exploiting the AE. The AERONET AOD at 470 nm was calculated using the AERONET AOD at 440 nm and AE at 440-870 nm. Similarly, the SKYNET AOD at 470 nm was computed using the SKYNET AOD at 400 nm and AE at 400-1020 nm. The NO₂-modified AERONET and SKYNET AOD at 470 nm were also computed using the same approach and the modified AOD and AE retrievals.



We observe a generally satisfactory agreement between the ground-based (both AERONET and SKYNET) and MODIS DB
410 AOD data with a Pearson correlation (r) higher than 0.7. In general, MODIS DB AOD slightly overestimates the AOD
observed by the sun-photometers. The bias (calculated as satellite minus sun-photometer AOD) between MODIS DB and the
different ground-based data sets before the correction (upper panels of Fig. 10) varies from -0.009 for SKYNET APL-SAP
data (-0.008 considering AERONET) to 0.027 for AERONET CNR-ISAC. AERONET data, available for both sites, highlight
a lower agreement for the CNR-ISAC site, with a bias about 3 times larger with respect to the APL-SAP site. The correction
415 introduces a slight change of about 0.003 in the agreement between MODIS DB and AERONET AOD products and of 0.006
between MODIS and SKYNET data (lower panels of Fig. 10). Figure 10 also shows an improvement in the percentage of
MODIS AOD data falling within the expected error (EE) of $\pm (0.05 + 20 \%)$ (Hsu et al., 2013) for APL-SAP adopting the
correction on both AERONET and SKYNET.

In Fig. 11, we show the absolute correction (computed as the difference between original AERONET/SKYNET AOD data at
420 470 nm and modified ones) as a function of the MODIS DB AOD and the NO_2 column retrieved by the Pandora instruments
located at APL-SAP and CNR-ISAC sites. As already highlighted, we observe that the correction only depends on the NO_2
amount and not on the AOD. Figure 11 also highlights that, although the improvement is relatively slight on average, the
correction can be larger than 10/15% in many cases.

This inter-comparison exercise demonstrated that the proposed correction improves the agreement between MODIS DB AOD
425 data and AERONET and SKYNET AOD products. Since the proposed correction depends on the amount of NO_2 , the
improvement is more significant in the correspondence of high values of NO_2 , typical of highly polluted areas such as the
urban area of Rome (APL-SAP). Nevertheless, a slight improvement is achieved also in the suburban area of Rome (CNR-
ISAC).

3.6 Impact on SSA

430 One of the main impacts of accurate characterization of the column NO_2 concentration is certainly expected on the retrieved
values of SSA in spectral ranges coinciding with NO_2 absorptions. In order to quantify this effect, the sensitivity of AERONET
retrieval of SSA at 440 nm has been tested. For that purpose, the Generalized Retrieval of Atmosphere and Surface Properties
(GRASP) algorithm (Dubovik et al., 2021) was applied to the standard AERONET aerosol retrieval measurements (TOD and
almucantar at 440, 675, 870 and 1020 nm) following two different approaches. First, the reference for these comparisons was
435 established by using GRASP retrieval configured as closely as possible to mimic the AERONET operational retrieval.
Specifically, the NO_2 absorption values were taken from the same source as done in the AERONET processing (OMI
climatology). On the other hand, GRASP is very flexible and allows the use of different assumptions of the gaseous properties.
Therefore, in addition to the standard approach, the accurate aerosol retrieval has been done by using the total columnar NO_2
concentrations provided by the Pandora spectrometers co-located with AERONET instruments at the two stations selected for
440 this study. Thus, in addition to the standard AERONET retrieval, GRASP has provided aerosol retrieval using these more
accurate NO_2 concentrations. The NO_2 absorption features were estimated more precisely from those concentrations by using



a K-Distribution approach; the “k bin” code (Doppler et al., 2014a; Doppler et al., 2014b) has been used to speed up the calculations.

The comparisons of the SSA at 440 nm obtained with GRASP/AERONET NO₂ and GRASP/Pandora NO₂ improved
445 absorption features for the two stations for the complete data set (not shown) do not show a clear influence of the change of
NO₂ concentration. High correlations ($r^2 > 0.98$) and a Mean Bias Error (MBE < 0.002) very close to zero are obtained. The
mean NO₂ column concentration for the retrievals presented here is 0.4 DU. Thus, in general the analysed improvements are
not expected to produce an important change in the retrieved parameters at 440 nm in the conditions with relatively low NO₂
absorption. However, in the cases where NO₂ concentration is elevated compared to climatological expected range, significant
450 changes in the SSA at 440 nm retrievals can be appreciated. Figure 12 shows the comparisons of the SSA at 440 nm obtained
with GRASP following an AERONET-like approach (X-axis) and the approach with the new NO₂ concentrations provided by
Pandora (Y-axis), filtered for NO₂ concentrations higher than 0.9 DU. The two stations are correspondingly represented in the
left and right panels. As it can be noted, for both stations in conditions of high NO₂ concentrations there is a consistent positive
bias of 0.02 (2.5 %). However, a high correlation ($r^2 > 0.95$) and Root Mean Square Errors (RMSE < 0.035) are also observed.
455 Previous studies, regarding SSA retrieval uncertainty, found it in the range of 0.02-0.03 (Eck et al., 2003; Corr et al., 2009;
Jethva et al., 2014; Kazadzis et al., 2016), whereas the correction when high NO₂ is recorded, is usually higher. Thus, it is
clear that in conditions of high NO₂ concentrations an accurate characterization of this gas is necessary in order to avoid
noticeable bias in the affected AERONET channel around 440 nm.

4 Summary and conclusions

460 The retrievals of aerosol properties from sun-photometers may be significantly affected by NO₂ absorption in the observed
spectral range and, thus, the accurate assumptions on NO₂ concentrations are highly desirable. Currently, some ground-based
aerosol networks, such as SKYNET, do not take NO₂ optical depth into consideration in AOD retrieval processes, while others
(e.g., AERONET) use satellite-based NO₂ climatology for estimating it. However, quite significant errors may be introduced
in the AOD retrievals, especially over urban areas, where NO₂ is characterized by rather short lifetime and high spatial and
465 temporal variations, due to inhomogeneous local emission patterns and photochemical destruction.

Actual co-located surface-based NO₂ measurements (e.g., from Pandora instruments) or space-borne observations with
improved spatial and temporal resolution (e.g., S5P/TROPOMI) may be helpful for reducing the uncertainty of the NO₂ optical
depth contribution in later versions of AOD retrieval algorithms. In this study, we evaluated the possible improvements of
AOD and AE retrievals by applying a specific correction using synchronous and co-located measurements of total NO₂ column
470 from Pandora spectroradiometers and the TROPOMI satellite sensor. For this purpose, we used multiannual (2017-2022)
observations from both AERONET and SKYNET multispectral AOD observations co-located with Pandora instruments and
collected over two locations in Rome (Italy) with different anthropic pressure, one in the city centre and the other in a suburban
area.



The deviations of the NO₂-modified AOD retrievals from the network standard products were investigated. The impact of the
475 correction is higher in the case of SKYNET since the NO₂ optical depth is not considered at all in the standard retrieval
processes. At the same time, the observed differences in the results between the two networks can be partly explained also by
the different channels used for the retrievals. Although in most of the cases the differences are lower than 0.01 for AOD and
lower than 0.1 for AE retrievals, the correction can be still useful for lower AODs (< 0.3), where the majority of observations
is found, especially under high NO₂ pollution events. As expected, the effect of improved NO₂ assumption in the retrievals is
480 more evident in both AOD and AE when the actual synchronous ground-based Pandora NO₂ measurements are employed
compared to the situations when the used correction was based on daily or monthly averaged Pandora data or TROPOMI NO₂
retrievals. In addition, AERONET-used NO₂ climatology was found to systematically underestimate Pandora-measured NO₂
over both sites.

In addition, a first attempt to evaluate the impact of those corrections to AOD and AE annual trends was conducted. However,
485 the aerosol data sets employed in this trend analysis are quite short for a statistically meaningful trend analysis. Although the
effect of NO₂ on the derived trends seems to be insignificant and the linear fit trend calculations introduce uncertainties similar
or higher to the NO₂ effects on AOD, the more pronounced impact may be expected for trends derived from larger data sets
as well as in the case of a significant NO₂ trend.

We also investigated the possible effects of the proposed NO₂ optical depth correction on the agreement of MODIS DB AOD
490 retrievals at 470 nm with AERONET and SKYNET AOD products. In general, the agreement between ground-based (both
AERONET and SKYNET) and MODIS DB AOD is quite good, revealing a correlation coefficient (r) higher than 0.7. The use
of Pandora NO₂ in the sun-photometers retrievals introduces a slight improvement in absolute values of ~ 0.003 in the
agreement between MODIS DB and AERONET AOD and an improvement of ~ 0.006 between MODIS and SKYNET
observations. Although the impact on the comparisons between space-borne and ground-based observations of AOD is quite
495 small, it can be quite useful for eliminating or decreasing possible biases in the inter-comparisons of satellite and ground-based
data in situations with NO₂ concentrations typical for highly polluted areas.

Moreover, we investigated the impact of using a precise characterization of the total NO₂ concentration on the SSA retrieval
at 440 nm from AERONET measurements. For this, the GRASP algorithm was used to evaluate the effect of NO₂ correction
on AERONET aerosol retrievals obtained by inverting TOD and almucantar radiances at 440, 675, 870 and 1020 nm. GRASP
500 aerosol retrieval using the actual total NO₂ concentration provided by the co-located Pandora, over both stations selected for
this study, were compared with GRASP retrievals mimicking AERONET operational retrievals. The results showed that, in
general, the effect in the retrieved parameters at 440 nm under low NO₂ absorption conditions was not significant. At the same
time, for the cases with high NO₂ loadings (> 0.9 DU) important changes in the retrieved SSA were observed, with an average
positive bias of 0.02 (2.5 %) for both locations.

505 In general, NO₂ absorption is very important to account in the retrieval of aerosol properties especially AE, AOD and SSA at
440 nm. Moreover, if NO₂ absorption is accounted from climatological data, the accuracy of such approach may not be
sufficient at locations where NO₂ has high diurnal variability during high NO₂ concentration episodes that cannot be captured



510 by the satellite climatology. In such situations the use of accurate co-located NO₂ observations, e.g., by Pandora instruments, is highly desirable. Thus, based on results of this study, the effect of NO₂ correction could be considered relatively small for large fraction of the observations, nonetheless the correction has certainly contributed towards lowering the uncertainty of AOD and, especially, aerosol SSA provided by sun-photometers.

515 Finally, the improved technology including real-time NO₂ monitoring (e.g., the Pandonia network), real-time satellite-based products at high spatial resolution (e.g., TROPOMI) and the foreseen more precise NO₂ products (e.g., from Sentinel 4) tend to positively contribute towards improving retrieved aerosol properties in the spectral range (~380 – 440 nm) affected by NO₂ absorption.

Data availability. The AOD and AE products from the CIMEL sunphotometer measurements as well as the NO₂ optical depth used in the retrievals are available in the AERONET data server (<http://aeronet.gsfc.nasa.gov/>). The SKYNET AOD and AE data sets were downloaded from the international SKYNET data center (<https://www.skynet-isdc.org/data.php>). The Pandora total NO₂ columns are available in the Pandonia Global Network website (<https://www.pandonia-global-network.org/>). The S5P/TROPOMI NO₂ products were obtained from the Sentinel-5P Pre-Operations Data Hub of the Copernicus Open Access Hub (<https://scihub.copernicus.eu/>). The MODIS DB products are available at the Level-1 and Atmosphere Archive and Distribution System Distributed Active Archive Center (<http://ladsweb.nascom.nasa.gov>). The SSA retrievals from the CIMEL almucantar measurements can be accessed by contacting the author.

525 *Author contribution.* The manuscript was prepared by TD, I-PR, and MV. TD and I-PR developed and implemented the correction algorithm for AOD and AE retrievals and conducted the trend analysis. MV and SC conducted the inter-comparison of ground-based AOD with MODIS DB products and performed the S5P/TROPOMI data extraction and visualization. MH-G and AL developed the SSA retrieval algorithm and conducted the analysis on SSA results. SC, FB and MC supervised the maintenance and operation of ground-based instruments as well as the acquisition and curation of the respective data sets. OD contributed in the discussions on the SSA analysis and the inter-comparisons with MODIS DB. I-PR, SK, GB and FN supervised the investigation and contributed towards methodological ideas and their presentation. All authors reviewed and edited the manuscript.

535 *Competing interests.* The authors declare that they have no conflict of interest.

Acknowledgements. The work has been supported by the European Space Agency (ESA) in the frame of the Instrument Data quality Evaluation and Assessment Service - Quality Assurance for Earth Observation (IDEAS-QA4EO) project. OD and SK acknowledge the European Metrology Program for Innovation and Research (EMPIR) within the joint research project EMPIR MAPP: “Metrology for aerosol optical properties”. The EMPIR is jointly funded by the EMPIR participating countries within



EURAMET and the European Union. SK would like to acknowledge the ACTRIS Switzerland project funded by the Swiss State Secretariat for Education Research and Innovation.



References

- 545 Arola, A., and Koskela, T.: On the sources of bias in aerosol optical depth retrieval in the UV range, *J. Geophys. Res.*, 109, D08209, doi:10.1029/2003JD004375, 2004.
- Bellini, A., Diémoz, H., Di Liberto, L., Gobbi, G.P., and Barnaba, F.: Monitoring the aerosol vertical profiles within the Italian Automated Lidar-Ceilometer network (Alicenet): retrievals and applications for air quality and multi risk-warning systems, in preparation, 2023.
- 550 Benedetti, A., Reid, J. S., Knippertz, P., Marsham, J. H., Di Giuseppe, F., Rémy, S., Basart, S., Boucher, O., Brooks, I. M., Menut, L., Mona, L., Laj, P., Pappalardo, G., Wiedensohler, A., Baklanov, A., Brooks, M., Colarco, P. R., Cuevas, E., da Silva, A., Escribano, J., Flemming, J., Huneus, N., Jorba, O., Kazadzis, S., Kinne, S., Popp, T., Quinn, P. K., Sekiyama, T. T., Tanaka, T., and Terradellas, E.: Status and future of numerical atmospheric aerosol prediction with a focus on data requirements, *Atmos. Chem. Phys.*, 18, 10615-10643, <https://doi.org/10.5194/acp-18-10615-2018>, 2018.
- 555 Boersma, K. F., Eskes, H. J., and Brinksma, E. J.: Error analysis for tropospheric NO₂ retrieval from space, *J. Geophys. Res.*, 109, D04311, doi:10.1029/2003JD003962, 2004.
- Boersma, K. F., Jacob, D. J., Eskes, H. J., Pinder, R. W., Wang, J., and van der A, R. J.: Inter-comparison of SCIAMACHY and OMI tropospheric NO₂ columns: Observing the diurnal evolution of chemistry and emissions from space, *J. Geophys. Res.*, 113, 1–14, doi:10.1029/2007JD008816, 2008.
- 560 Boersma, K. F., Eskes, H. J., Dirksen, R. J., van der A, R. J., Veeckind, J. P., Stammes, P., Huijnen, V., Kleipool, Q. L., Sneep, M., Claas, J., Leitão, J., Richter, A., Zhou, Y., and Brunner, D.: An improved tropospheric NO₂ column retrieval algorithm for the Ozone Monitoring Instrument, *Atmos. Meas. Tech.*, 4, 1905–1928, <https://doi.org/10.5194/amt-4-1905-2011>, 2011.
- Burrows, J.P., Dehn, A., Deters, B., Himmelmann, S., Richter, A., Voigt, S., and Orphal, J.: Atmospheric remote-sensing reference data from GOME: Part 1. Temperature-dependent absorption cross-sections of NO₂ in the 231-794 nm range" *J. Quant. Spectrosc. Radiat. Transfer*, 60, 1025-1031, 1998.
- 565 Campanelli, M., Nakajima, T., and Olivieri, B.: Determination of the solar calibration constant for a sun-sky radiometer: proposal of an in-situ procedure, *Appl. Opt.* 43, 651-659, 2004.
- Campanelli, M., Iannarelli, A.M., Mevi, G., Casadio, S., Diémoz, H., Finardi, S., Dinoi, A., Castelli, E., di Sarra, A., Di Bernardino, A., Casasanta, G., Bassani, C., Siani, A.M., Cacciani, M., Barnaba, F., Di Liberto, L., Argentini, S.: A wide-
- 570 ranging investigation of the COVID-19 lockdown effects on the atmospheric composition in various Italian urban sites (AER – LOCUS), *Urban Climate*, Volume 39, 100954, ISSN 2212-0955, <https://doi.org/10.1016/j.uclim.2021.100954>, 2021.
- Cede, A., Tiefengraber, M., Dehn, A., Lefer, B., von Bismarck, J., Casadio, S., Abuhassan, N., Swap, R., and Valin, L.: Operational satellite validation with data from the Pandonia Global Network (PGN), EGU General Assembly 2020, Online, 575 4–8 May 2020, EGU2020-13850, <https://doi.org/10.5194/egusphere-egu2020-13850>, 2020.



- Cede, A.: Manual for Blick Software Suite 1.8, 10 Sep 2021, Issue 1.8-4, available at: https://www.pandonia-global-network.org/wp-content/uploads/2021/09/BlickSoftwareSuite_Manual_v1-8-4.pdf (last access: 22 April 2022), 2021.
- Chu, D., Kaufman, Y. J., Ichoku, C., Remer, L., Tanre, D., and Holben, B. N.: Validation of MODIS aerosol optical depth retrieval over land, *Geophys. Res. Lett.*, 29(12), 1617, doi:10.1029/2001GL013205, 2002.
- 580 Ciardini, V., Di Iorio, T., Di Liberto, L., Tirelli, C., Casasanta, G., di Sarra, A., Fiocco, G., Fuà, D., and Cacciani, M.: Seasonal variability of tropospheric aerosols in Rome, *Atmos. Res.*, 118, 205–214, <https://doi.org/10.1016/j.atmosres.2012.06.026>, 2012.
- Corr, C. A., Krotkov, N., Madronich, S., Slusser, J. R., Holben, B., Gao, W., Flynn, J., Lefer, B., and Kreidenweis, S. M.: Retrieval of aerosol single scattering albedo at ultraviolet wavelengths at the T1 site during MILAGRO, *Atmos. Chem. Phys.*, 9, 5813–5827, doi:10.5194/acp-9-5813-2009, 2009.
- 585 Di Bernardino, A., Iannarelli, A. M., Casadio, S., Mevi, G., Campanelli, M., Casasanta, G., Cede, A., Tiefengraber, M., Siani, A. M., Spinei, E., and Cacciani, M.: On the effect of sea breeze regime on aerosols and gases properties in the urban area of Rome, Italy, *Urban Climate*, 37, 100842, <https://doi.org/10.1016/j.uclim.2021.100842>, 2021.
- Di Ianni A, Costabile F, Barnaba F, Di Liberto L, Weinhold K, Wiedensohler A, Struckmeier C, Drewnick F, Gobbi GP.: Black Carbon Aerosol in Rome (Italy): Inference of a Long-Term (2001–2017) Record and Related Trends from AERONET Sun-Photometry Data. *Atmosphere*. 9(3), 81, <https://doi.org/10.3390/atmos9030081>, 2018.
- 590 Di Tomaso, E., Escribano, J., Basart, S., Ginoux, P., Macchia, F., Barnaba, F., Benincasa, F., Bretonnière, P.-A., Buñuel, A., Castrillo, M., Cuevas, E., Formenti, P., Gonçalves, M., Jorba, O., Klose, M., Mona, L., Montané Pinto, G., Mytilinaios, M., Obiso, V., Olid, M., Schutgens, N., Votsis, A., Werner, E., and Pérez García-Pando, C.: The MONARCH high-resolution reanalysis of desert dust aerosol over Northern Africa, the Middle East and Europe (2007–2016), *Earth Syst. Sci. Data*, 14, 2785–2816, <https://doi.org/10.5194/essd-14-2785-2022>, 2022.
- 595 Diémoz, H., Siani, A. M., Casadio, S., Iannarelli, A. M., Casale, G. R., Savastiouk, V., Cede, A., Tiefengraber, M., and Müller, M.: Advanced NO₂ retrieval technique for the Brewer spectrophotometer applied to the 20-year record in Rome, Italy, *Earth Syst. Sci. Data*, 13, 4929–4950, <https://doi.org/10.5194/essd-13-4929-2021>, 2021.
- 600 Doppler, L., Carbajal-Henken, C., Pelon, J., Ravetta, F., and Fischer, J.: Extension of radiative transfer code MOMO, matrix-operator model to the thermal infrared—Clear air validation by comparison to RTTOV and application to CALIPSO-IIR. *Journal of Quantitative Spectroscopy and Radiative Transfer*, 144, 49–67, 2014a.
- Doppler, L., Preusker, R., Bennartz, R., and Fischer, J.: k-bin and k-IR: k-distribution methods without correlation approximation for non-fixed instrument response function and extension to the thermal infrared—Applications to satellite remote sensing. *Journal of Quantitative Spectroscopy and Radiative Transfer*, 133, 382–395, 2014b.
- 605 Drosoglou, T., Bais, A. F., Zyrichidou, I., Kouremeti, N., Poupkou, A., Liora, N., Giannaros, C., Koukouli, M. E., Balis, D., and Melas, D.: Comparisons of ground-based tropospheric NO₂ MAX-DOAS measurements to satellite observations with the aid of an air quality model over the Thessaloniki area, Greece, *Atmos. Chem. Phys.*, 17, 5829–5849, <https://doi.org/10.5194/acp-17-5829-2017>, 2017.



- 610 Dubovik, O. and King, M. D.: A flexible inversion algorithm for retrieval of aerosol optical properties from Sun and sky radiance measurements, *J. Geophys. Res.*, 105, 20,673-20,696, 2000.
- Dubovik, O., Smirnov, A., Holben, B. N., King, M. D., Kaufman, Y. J., Eck, T. F., and Slutsker, I.: Accuracy assessments of aerosol optical properties retrieved from AERONET Sun and sky-radiance measurements, *J. Geophys. Res.*, 105, 9791-9806, 2000.
- 615 Dubovik, O., Holben, B. N., Eck, T. F., Smirnov, A., Kaufman, Y. J., King, M. D., Tanré, D., and Slutsker, I.: Variability of absorption and optical properties of key aerosol types observed in worldwide locations, *J. Atmos. Sci.*, 59, 590-608, 2002.
- Dubovik, O., Fuertes, D., Litvinov, P., Lopatin, A., Lapyonok, T., Dubovik, I., et al.: A comprehensive description of multi-term LSM for applying multiple a priori constraints in problems of atmospheric remote sensing: GRASP algorithm, concept, and applications. *Front. Remote Sens*, 2021.
- 620 Eck T. F., Holben, B. N., Reid, J. S., Dubovik, O., Kinne, S., Smirnov, A., O'Neill, N. T., and Slutsker, I.: The wavelength dependence of the optical depth of biomass burning, urban and desert dust aerosols, *J. Geophys. Res.*, 104, 31,333-31,350, 1999.
- Eck, T. F., Holben, B. N., Ward, D. E., Mukelabai, M. M., Dubovik, O., Smirnov, A., Schafer, J. S., Hsu, N. C., Piketh, S. J., Queface, A., and Roux, J. L.: Variability of biomass burning aerosol optical characteristics in southern Africa during the
- 625 SAFARI 2000 dry season campaign and a comparison of single scattering albedo estimates from radiometric measurements, *J. Geophys. Res.-Atmos.*, 108, 2156–2202, doi:10.1029/2002JD002321, 2003.
- Eskes, H., van Geffen, J., Boersma, F., Eichmann, K.-U., Apituley, A., Pedergnana, M., Sneep, M., Veeffkind, J. P., and Loyola, D.: Sentinel-5 precursor/TROPOMI Level 2 Product User Manual Nitrogen dioxide, Tech. Rep. S5PKNMI-L2-0021-MA, Koninklijk Nederlands Meteorologisch Instituut (KNMI), CI-7570-PUM, issue 4.1.0, available at:
- 630 <https://sentinel.esa.int/documents/247904/2474726/Sentinel-5P-Level-2-Product-User-Manual-Nitrogen-Dioxide.pdf> (last access: 21 October 2022), 2022.
- Eskes, H. J. and Eichmann, K.-U.: S5P Mission Performance Centre Nitrogen Dioxide [L2_NO2___] Readme, issue 2.2, version 02.04.00, 21 pp., 17 November 2021, available at: <https://sentinel.esa.int/documents/247904/3541451/Sentinel-5P-Nitrogen-Dioxide-Level-2-Product-Readme-File> (last access: 21 October 2022), 2022.
- 635 Estellés, V., Campanelli, M., Smyth, T. J., Utrillas, M. P., and Martínez-Lozano, J. A.: Evaluation of the new ESR network software for the retrieval of direct sun products from CIMEL CE318 and PREDE POM01 sun-sky radiometers, *Atmos. Chem. Phys.*, 12, 11619–11630, <https://doi.org/10.5194/acp-12-11619-2012>, 2012.
- Fan, C., Li, Z., Li, Y., Dong, J., van der A, R., and de Leeuw, G.: Variability of NO₂ concentrations over China and effect on air quality derived from satellite and ground-based observations, *Atmos. Chem. Phys.*, 21, 7723–7748, <https://doi.org/10.5194/acp-21-7723-2021>, 2021.
- 640 Flynn, C. M., Pickering, K. E., Crawford, J. H., Lamsal, L., Krotkov, N., Herman, J., Weinheimer, A., Chen, G., Liu, X., Szykman, J., Tsay, S.-C., Loughner, C., Hains, J., Lee, P., Dickerson, R. R., Stehr, J. W., and Brent, L.: Relationship



- between column-density and surface mixing ratio: Statistical analysis of O₃ and NO₂ data from the July 2011 Maryland DISCOVER-AQ mission, *Atmos. Environ.*, 92, 429–441, <https://doi.org/10.1016/j.atmosenv.2014.04.041>, 2014.
- 645 Giles, D. M., Sinyuk, A., Sorokin, M. G., Schafer, J. S., Smirnov, A., Slutsker, I., Eck, T. F., Holben, B. N., Lewis, J. R., Campbell, J. R., Welton, E. J., Korkin, S. V., and Lyapustin, A. I.: Advancements in the Aerosol Robotic Network (AERONET) Version 3 database – automated near-real-time quality control algorithm with improved cloud screening for Sun photometer aerosol optical depth (AOD) measurements, *Atmos. Meas. Tech.*, 12, 169–209, <https://doi.org/10.5194/amt-12-169-2019>, 2019.
- 650 Gkikas, A., Proestakis, E., Amiridis, V., Kazadzis, S., Di Tomaso, E., Tsekeri, A., Marinou, E., Hatzianastassiou, N., and Pérez García-Pando, C.: ModIs Dust AeroSol (MIDAS): a global fine-resolution dust optical depth data set, *Atmos. Meas. Tech.*, 14, 309–334, <https://doi.org/10.5194/amt-14-309-2021>, 2021.
- Gobbi, G.P., Angelini F., Barnaba F., Costabile F., Baldasano J.M., Basart S., Sozzi R., Bolignano A.: Changes in particulate matter physical properties during Saharan advections over Rome (Italy): a four-year study, 2001–2004. *Atmos Chem Phys* 13:7395–7404. <https://doi.org/10.5194/acp-13-7395-2013>, 2017.
- 655 Green, M, Kondragunta, S, Ciren, P, Xu, C.: Comparison of GOES and MODIS aerosol optical depth (AOD) to aerosol robotic network (AERONET) AOD and IMPROVE PM_{2.5} mass at Bondville, Illinois, *J Air Waste Manag Assoc.*, 59(9):1082-91, doi: 10.3155/1047-3289.59.9.1082, 2009.
- Herman, J., Cede, A., Spinei, E., Mount, G., Tzortziou, M., and Abuhassan, N.: NO₂ column amounts from ground-based Pandora and MFDOAS spectrometers using the direct-sun DOAS technique: Intercomparisons and application to OMI validation, *J. Geophys. Res.*, 114, D13307, doi:10.1029/2009JD011848, 2009.
- 660 Herman, J., Spinei, E., Fried, A., Kim, J., Kim, J., Kim, W., Cede, A., Abuhassan, N., and Segal-Rozenhaimer, M.: NO₂ and HCHO measurements in Korea from 2012 to 2016 from Pandora spectrometer instruments compared with OMI retrievals and with aircraft measurements during the KORUS-AQ campaign, *Atmos. Meas. Tech.*, 11, 4583–4603, <https://doi.org/10.5194/amt-11-4583-2018>, 2018.
- 665 Hobbs, P. V.: Aerosol-cloud interactions, in: *Aerosol-Cloud-Climate Interactions*, Academic, San Diego, California, 1993.
- Holben, B.N., Eck, T.F., Slutsker, I.A., Tanre, D., Buis, J.P., Setzer, A., Vermote, E., et al.: AERONET—A federated instrument network and data archive for aerosol characterization, *Remote Sens. Environ.* 66 (1), 1–16, 1998.
- Hsu, N. C., Tsay, S.-C., King, M. D., and Herman, J. R.: Aerosol Properties Over Bright-Reflecting Source Regions, *IEEE T. Geosci. Remote Sens.*, 42, 557–569, <https://doi.org/10.1109/TGRS.2004.824067>, 2004.
- 670 Hsu, N. C., Tsay, S.-C., King, M. D., and Herman, J. R.: Deep Blue Retrievals of Asian Aerosol Properties During ACE-Asia, *IEEE T. Geosci. Remote S.*, 44, 3180–3195, <https://doi.org/10.1109/TGRS.2006.879540>, 2006.
- Hsu, N. C., Jeong, M.-J., Bettenhausen, C., Sayer, A. M., Hansell, R., Seftor, C. S., Huang, J., and Tsay, S.-C.: Enhanced Deep Blue aerosol retrieval algorithm: The second generation, *J. Geophys. Res.-Atmos.*, 118, 9296–9315, <https://doi.org/10.1002/jgrd.50712>, 2013.
- 675



- Iannarelli, A. M., Di Bernardino, A., Casadio, S., Bassani, C., Cacciani, M., Campanelli, M., Casasanta, G., Cadau, E., Diémoz, H., Mevi, G., Siani, A. M., Cardaci, M., Dehn, A., and Goryl, P.: The Boundary Layer Air Quality-Analysis Using Network of Instruments (BAQUNIN) Supersite for Atmospheric Research and Satellite Validation over Rome Area, *B. Am. Meteorol. Soc.*, E599–E618, <https://doi.org/10.1175/BAMS-D-21-0099.1>, 2021.
- 680 IPCC: Climate Change 2013: The Physical Science Basis. Contribution of Working Group I to the Fifth Assessment Report of the Intergovernmental Panel on Climate Change, edited by: Stocker, T. F., Qin, D., Plattner, G.-K., Tignor, M., Allen, S. K., Boschung, J., Nauels, A., Xia, Y., Bex, V., and Midgley, P. M., Cambridge University Press, Cambridge, United Kingdom and New York, NY, USA, 1535 pp., 2013.
- ISTAT: Annual demographic balance 2021,
685 <http://demo.istat.it/bilmens/query.php?anno=2021&lingua=ita&Rip=S3&Reg=R12&Pro=P058&Com=91&submit=Tavola>, (last access: 21 August 2022), 2021.
- Jethva, H., Torres, O., and Ahn, C.: Global assessment of OMI aerosol single-scattering albedo using ground-based AERONET inversion, *J. Geophys. Res.-Atmos.*, 119, 9020–9040, doi:10.1002/2014JD021672, 2014.
- Kazadzis, S., Raptis, P., Kouremeti, N., Amiridis, V., Arola, A., Gerasopoulos, E., and Schuster, G. L.: Aerosol absorption
690 retrieval at ultraviolet wavelengths in a complex environment, *Atmos. Meas. Tech.*, 9, 5997–6011, <https://doi.org/10.5194/amt-9-5997-2016>, 2016.
- Kazadzis, S., Kouremeti, N., Nyeki, S., Gröbner, J., and Wehrli, C.: The World Optical Depth Research and Calibration Center (WORCC) quality assurance and quality control of GAW-PFR AOD measurements, *Geosci. Instrum. Method. Data Syst.*, 7, 39–53, <https://doi.org/10.5194/gi-7-39-2018>, 2018a.
- 695 Kazadzis, S., Kouremeti, N., Diémoz, H., Gröbner, J., Forgan, B. W., Campanelli, M., Estellés, V., Lantz, K., Michalsky, J., Carlund, T., Cuevas, E., Toledano, C., Becker, R., Nyeki, S., Kosmopoulos, P. G., Tatsiankou, V., Vuilleumier, L., Denn, F. M., Ohkawara, N., Ijima, O., Goloub, P., Raptis, P. I., Milner, M., Behrens, K., Barreto, A., Martucci, G., Hall, E., Wendell, J., Fabbri, B. E., and Wehrli, C.: Results from the Fourth WMO Filter Radiometer Comparison for aerosol optical depth measurements, *Atmos. Chem. Phys.*, 18, 3185–3201, <https://doi.org/10.5194/acp-18-3185-2018>, 2018b.
- 700 Kreher, K., Van Roozendaal, M., Hendrick, F., Apituley, A., Dimitropoulou, E., Frieß, U., Richter, A., Wagner, T., Lampel, J., Abuhassan, N., Ang, L., Anguas, M., Bais, A., Benavent, N., Bösch, T., Bogner, K., Borovski, A., Bruchkouski, I., Cede, A., Chan, K. L., Donner, S., Drosoglou, T., Fayt, C., Finkenzeller, H., Garcia-Nieto, D., Gielen, C., Gómez-Martín, L., Hao, N., Henzing, B., Herman, J. R., Hermans, C., Hoque, S., Irie, H., Jin, J., Johnston, P., Khayyam Butt, J., Khokhar, F., Koenig, T. K., Kuhn, J., Kumar, V., Liu, C., Ma, J., Merlaud, A., Mishra, A. K., Müller, M., Navarro-Comas, M.,
705 Ostendorf, M., Pazmino, A., Peters, E., Pinardi, G., Pinharanda, M., Piter, A., Platt, U., Postlyakov, O., Prados-Roman, C., Puentedura, O., Querel, R., Saiz-Lopez, A., Schönhardt, A., Schreier, S. F., Seyler, A., Sinha, V., Spinei, E., Strong, K., Tack, F., Tian, X., Tiefengraber, M., Tirpitz, J.-L., van Gent, J., Volkamer, R., Vrekoussis, M., Wang, S., Wang, Z., Wenig, M., Wittrock, F., Xie, P. H., Xu, J., Yela, M., Zhang, C., and Zhao, X.: Intercomparison of NO₂, O₄, O₃ and HCHO



- 710 slant column measurements by MAX-DOAS and zenith-sky UV–visible spectrometers during CINDI-2, *Atmos. Meas. Tech.*, 13, 2169–2208, <https://doi.org/10.5194/amt-13-2169-2020>, 2020.
- Lamsal, L. N., Janz, S. J., Krotkov, N. A., Pickering, K. E., Spurr, R. J. D., Kowalewski, M. G., Loughner, C. P., Crawford, J. H., Swartz, W. H., and Herman, J. R.: High-resolution NO₂ observations from the Airborne Compact Atmospheric Mapper: Retrieval and validation, *J. Geophys. Res.*, 122, 1953–1970, <https://doi.org/10.1002/2016JD025483>, 2017.
- 715 Lelieveld, J., Evans, J. S., Fnais, M., Giannadaki, D., and Pozzer, A.: The contribution of outdoor air pollution sources to premature mortality on a global scale, *Nature*, 525, 367–371, <https://doi.org/10.1038/nature15371>, 2015.
- Levy, R. C., Remer, L. A., Kleidman, R. G., Mattoo, S., Ichoku, C., Kahn, R., and Eck, T. F.: Global evaluation of the Collection 5 MODIS dark-target aerosol products over land, *Atmos. Chem. Phys.*, 10, 10399–10420, doi:10.5194/acp-10-10399-2010, 2010.
- 720 Levy, R. C., Mattoo, S., Munchak, L. A., Remer, L. A., Sayer, A. M., Patadia, F., and Hsu, N. C.: The Collection 6 MODIS aerosol products over land and ocean, *Atmos. Meas. Tech.*, 6, 2989–3034, <https://doi.org/10.5194/amt-6-2989-2013>, 2013.
- Li, J., Carlson, B. E., Lacis, A. A.: How well do satellite AOD observations represent the spatial and temporal variability of PM_{2.5} concentration for the United States?, *Atmospheric Environment*, Volume 102, Pages 260-273, ISSN 1352-2310, <https://doi.org/10.1016/j.atmosenv.2014.12.010>, 2015.
- 725 Logothetis, S.-A., Salamalikis, V., Gkikas, A., Kazadzis, S., Amiridis, V., and Kazantzidis, A.: 15-year variability of desert dust optical depth on global and regional scales, *Atmos. Chem. Phys.*, 21, 16499–16529, <https://doi.org/10.5194/acp-21-16499-2021>, 2021.
- Martins, D. K., Najjar, R. G., Tzortziou, M., Abuhassan, N., Thompson, A. M., and Kollonige, D. E.: Spatial and temporal variability of ground and satellite column measurements of NO₂ and O₃ over the Atlantic Ocean during the Deposition of Atmospheric Nitrogen to Coastal Ecosystems Experiment, *J. Geophys. Res.*, 121, 14175–14187, <https://doi.org/10.1002/2016JD024998>, 2016.
- 730 Molina, C., Toro A., R., Manzano, C.A., Canepari, S., Massimi, L., Leiva-Guzmán, M.A. Airborne Aerosols and Human Health: Leapfrogging from Mass Concentration to Oxidative Potential. *Atmosphere*, 11, 917. <https://doi.org/10.3390/atmos11090917>, 2020.
- 735 Müller, M., Gebetsberger, M., Tiefenraber, M., and Cede, A.: LuftBlick Report 2019003, Fiducial Reference Measurements for Air Quality, Calibration Procedures Document, Tech. rep., LuftBlick, https://www.pandonia-global-network.org/wp-content/uploads/2021/01/LuftBlick_FRM4AQ_CPD_RP_2019003_v4.0.pdf (last access: 22 April 2022), 2020.
- Nakajima, T., Tonna, G. and Rao, R., Boi, P., Kaufman, Y., Holben, B.: Use of sky brightness measurements from ground for remote sensing of particulate polydispersions, *Appl. Opt.*, 35, pp. 2672-2686, 1996.
- 740 Nakajima T., Campanelli, M., Che, H., Estellés, V., Irie, H., Kim, S.-W., Kim, J., Liu, D., Nishizawa, T., Pandithurai, G., Soni, V. K., Thana, B., Tugjurn, N.-U., Aoki, K., Go, S., Hashimoto, M., Higurashi, A., Kazadzis, S., Khatri, P., Kouremeti,



- N., Kudo, R., Marengo, F., Momoi, M., Ningombam, S. S., Ryder, C. L., Uchiyama, A., and Yamazaki, A.: An overview of and issues with sky radiometer technology and SKYNET, *AMT*, 13, 4195–4218, 2020.
- 745 Platt, U.: Differential optical absorption spectroscopy (DOAS), in: *Air Monitoring by Spectroscopic Techniques*, Chem. Anal. Ser. 127, John Wiley, New York, 27–84, 1994.
- Platt, U. and Stutz, J.: *Differential Optical Absorption Spectroscopy: Principles and Applications*, Springer, Germany, Berlin, 2008.
- Raptis, I.P., Kazadzis, S., Amiridis, V., Gkikas, A., Gerasopoulos, E., and Mihalopoulos, N.: A decade of aerosol optical properties measurements over Athens, Greece. *Atmosphere*, 11(2), p.154, 2020.
- 750 Remer, L., Kaufman, Y., Tanre, D., Mattoo, S., Chu, D., Martins, J., et al.: The MODIS aerosol algorithm, products, and validation, *J. Atmos. Sci.*, 62(4), 947–973, 2005.
- Richter, A., Burrows, J. P., Nüszlig, H., Granier, C., and Niemeier, U.: Increase in tropospheric nitrogen dioxide over China observed from space (and supplementary discussion on: Error estimates for changes in tropospheric NO₂ columns as derived from satellite measurements), *Nature*, 437, 129–132, doi:10.1038/nature04092, 2005.
- 755 Rosenfeld, D., Andreae, M.O., Asmi, A., Chin, M., de Leeuw, G., Donovan D.P., Kahn, R., Kinne, S., Kivekäs, N., Kulmala, M., Lau, W., Schmidt, K.S., Suni, T., Wagner, T., Wild, M., and Quaas, J.: Global observations of aerosol-cloud-precipitation-climate interactions, *Rev. Geophys.*, 52, 750–808, <https://doi.org/10.1002/2013RG000441>, 2014.
- Sherman, J.P., Gupta, P., Levy, R.C. and Sherman, P.J.: An Evaluation of MODIS-Retrieved Aerosol Optical Depth over a Mountainous AERONET Site in the Southeastern US. *Aerosol Air Qual. Res.* 16: 3243–3255.
- 760 <https://doi.org/10.4209/aaqr.2015.09.0568>, 2016.
- Sinyuk, A., Holben, B. N., Eck, T. F., Giles, D. M., Slutsker, I., Korkin, S., Schafer, J. S., Smirnov, A., Sorokin, M., and Lyapustin, A.: The AERONET Version 3 aerosol retrieval algorithm, associated uncertainties and comparisons to Version 2, *Atmos. Meas. Tech.*, 13, 3375–3411, <https://doi.org/10.5194/amt-13-3375-2020>, 2020.
- Solomon, S., Garcia, R. R., Rowland, F. S., and Wuebbles, D. J.: On the depletion of Antarctic ozone, *Nature*, 321, 755–758,
- 765 <https://doi.org/10.1038/321755a0>, 1986.
- Takamura T. and Nakajima T., Overview of SKYNET and its activities, *Opt. Pura Apl.* 37, 3303–3308, 2004.
- Tzortziou, M., Herman, J. R., Cede, A., and Abuhassan, N.: High precision, absolute total column ozone measurements from the Pandora spectrometer system: Comparisons with data from a Brewer double monochromator and Aura OMI. *Journal of Geophysical Research: Atmospheres*, 117(D16), 2012.
- 770 Tzortziou, M., Herman, J. R., Ahmad, Z., Loughner, C. P., Abuhassan, N., and Cede, A.: Atmospheric NO₂ dynamics and impact on ocean color retrievals in urban nearshore regions, *J. Geophys. Res.-Oceans*, 119, 3834–3854, <https://doi.org/10.1002/2014JC009803>, 2014.
- Tzortziou, M., Herman, J. R., Cede, A., Loughner, C. P., Abuhassan, N., and Naik, S.: Spatial and temporal variability of ozone and nitrogen dioxide over a major urban estuarine ecosystem, *J. Atmos. Chem.*, 72, 287–20 309,
- 775 <https://doi.org/10.1007/s10874-013-9255-8>, <https://doi.org/10.1007/s10874-013-9255-8>, 2015.



- Valentini, S., Barnaba, F., Bernardoni, V., Calzolari, G., Costabile, F., Di Liberto, L., Forello A.C., Gobbi, G.P., Gualtieri, M., Lucarelli F., Nava, S., Petralia, E., Valli, G., Wiedensohler, A., and Vecchi, R.: Classifying aerosol particles through the combination of optical and physical-chemical properties: Results from a wintertime campaign in Rome (Italy). *Atmospheric Research*, 235, 104799, 2020.
- 780 van Geffen, J. H. G. M., Boersma, K. F., Van Roozendaal, M., Hendrick, F., Mahieu, E., De Smedt, I., Sneep, M., and Veefkind, J. P.: Improved spectral fitting of nitrogen dioxide from OMI in the 405–465 nm window, *Atmos. Meas. Tech.*, 8, 1685–1699, <https://doi.org/10.5194/amt-8-1685-2015>, 2015.
- van Geffen, J.H.G.M.; Eskes, H.J.; Boersma, K.F.; Veefkind, J.P.: TROPOMI ATBD of the Total and Tropospheric NO₂ Data Products, available at: <https://sentinel.esa.int/documents/247904/2476257/Sentinel-5P-TROPOMI-ATBD-NO2-data-products> (last access: 21 October 2022), 2022.
- 785 Weatherhead, E. C., Reinsel, G.C., Tiao, G.C., Meng, X.-L., Choi, D., Cheang, W.-K., Keller, T., DeLuisi, J., Wuebbles, D.J., Kerr, J.B., Miller, A.J., Oltmans, S.J. and Frederick, J.E.: Factors affecting the detection of trends: Statistical considerations and applications to environmental data, *J. Geophys. Res.*, 103(D14), 17149–17161, doi:10.1029/98JD00995, 1998.
- 790 Wei, J., Li, Z., Peng, Y., Sun, L.: MODIS Collection 6.1 aerosol optical depth products over land and ocean: validation and comparison, *Atmos. Environ.*, 201, 428–440, <https://doi.org/10.1016/j.atmosenv.2018.12.004>, 2019.
- Yoon, J., von Hoyningen-Huene, W., Kokhanovsky, A. A., Vountas, M., and Burrows, J. P.: Trend analysis of aerosol optical thickness and Ångström exponent derived from the global AERONET spectral observations, *Atmos. Meas. Tech.*, 5, 1271–1299, <https://doi.org/10.5194/amt-5-1271-2012>, 2012.
- 795 Zhang, J. and Reid, J. S.: A decadal regional and global trend analysis of the aerosol optical depth using a data-assimilation grade over-water MODIS and Level 2 MISR aerosol products, *Atmos. Chem. Phys.*, 10, 10949–10963, <https://doi.org/10.5194/acp-10-10949-2010>, 2010.



Table 1. Deviation of Pandora total NO₂ column from satellite climatology used for AERONET retrievals and differences in modified AERONET and SKYNET AOD and AE from the standard products over CNR-ISAC and APL-SAP calculated using actual Pandora total NO₂ observations, as well as daily and monthly averaged values of NO₂. Note that the spectral channels used in AERONET retrievals are 380 and 440nm for AOD and 440-870nm for AE, whereas for SKYNET the wavelength channels are 400nm and 400-1020nm for AOD and AE, respectively.

	PGN NO ₂ Actual Measurements						PGN NO ₂ Daily Mean						PGN NO ₂ Monthly Mean					
	AERONET		AERONET		SKYNET		AERONET		AERONET		SKYNET		AERONET		AERONET		SKYNET	
	CNR-ISAC	APL-SAP	380	440	380	440	400	CNR-ISAC	APL-SAP	380	440	400	CNR-ISAC	APL-SAP	380	440	400	
NO₂	Channel [nm]		380	440	380	440	400			380	440	400			380	440	400	
	% Mean Deviation	61.23	64.81	63.51	64.51	-	-	53.22	57.21	65.30	66.37	-	45.45	49.63	59.41	60.716	-	
	Mean Deviation [DU]	0.163	0.168	0.162	0.163	-	-	0.141	0.147	0.167	0.169	-	0.120	0.127	0.151	0.153	-	
	STD [DU]	0.170	0.171	0.182	0.182	-	-	0.099	0.101	0.118	0.119	-	0.033	0.035	0.062	0.062	-	
	Minimum Deviation [DU]	1.3×10 ⁻⁵	0.3×10 ⁻⁵	2.83×10 ⁻⁶	0.6×10 ⁻⁶	-	-	0.6×10 ⁻⁵	0.7×10 ⁻⁵	0.1×10 ⁻⁵	0.5×10 ⁻⁵	-	0.6×10 ⁻⁶	0.004	0.010	0.012	-	
Maximum Deviation [DU]	2.066	2.080	2.406	2.410	-	-	0.803	0.815	0.773	0.777	-	0.297	0.311	0.291	0.293	-		
AOD	Channel [nm]	380	440	380	440	400	400	380	440	380	440	400	380	440	380	440	400	
	% Mean Deviation	1.512	1.695	1.677	1.682	5.275	5.275	1.330	1.510	1.886	1.897	5.597	1.164	1.344	1.844	1.814	5.681	
	Mean Deviation	0.0027	0.0024	0.0027	0.0024	0.0074	0.0074	0.0023	0.0021	0.0028	0.0024	0.0076	0.0020	0.0018	0.0025	0.0022	0.0074	
	STD	0.0028	0.0025	0.0030	0.0026	0.0034	0.0034	0.0016	0.0015	0.0020	0.0017	0.0022	0.0005	0.0004	0.0010	0.0009	0.0011	
	Minimum Deviation	0.02×10 ⁻⁶	0.05×10 ⁻⁶	0.04×10 ⁻⁶	0.09×10 ⁻⁷	0.0022	0.0022	0.01×10 ⁻⁵	0.01×10 ⁻⁵	0.02×10 ⁻⁶	0.07×10 ⁻⁶	0.0029	0.01×10 ⁻⁶	0.06×10 ⁻³	0.0002	0.0002	0.0052	
Maximum Deviation	0.034	0.030	0.040	0.035	0.043	0.043	0.013	0.012	0.013	0.011	0.018	0.005	0.004	0.005	0.004	0.010		
AE	Spectral Range [nm]	440-870	440-870	440-870	440-870	400-1020	400-1020	440-870	440-870	440-870	440-870	400-1020	440-870	440-870	440-870	440-870	400-1020	
	% Mean Deviation	1.731	2.552	2.552	2.552	6.960	6.960	1.415	1.415	2.696	2.696	7.559	1.178	1.178	2.895	2.895	7.938	
	Mean Deviation	0.019	0.021	0.021	0.021	0.053	0.053	0.016	0.016	0.022	0.022	0.057	0.012	0.012	0.021	0.021	0.058	
	STD	0.027	0.026	0.026	0.026	0.036	0.036	0.019	0.019	0.023	0.023	0.041	0.011	0.011	0.017	0.017	0.044	
	Minimum Deviation	0.02×10 ⁻⁶	0.01×10 ⁻⁶	0.01×10 ⁻⁶	0.01×10 ⁻⁶	0.002	0.002	0.08×10 ⁻⁵	0.08×10 ⁻⁵	0.01×10 ⁻⁴	0.01×10 ⁻⁴	0.002	0.12×10 ⁻⁵	0.12×10 ⁻⁵	0.04×10 ⁻⁵	0.04×10 ⁻⁵	0.003	
Maximum Deviation	0.309	0.291	0.291	0.291	0.701	0.701	0.215	0.215	0.322	0.322	0.621	0.139	0.139	0.248	0.248	0.640		



805 Table 2. Similar to Table 1, using TROPOMI measurements instead of Pandora total NO₂ for the estimation of NO₂ abundance in AERONET and SKYNET aerosol retrievals.

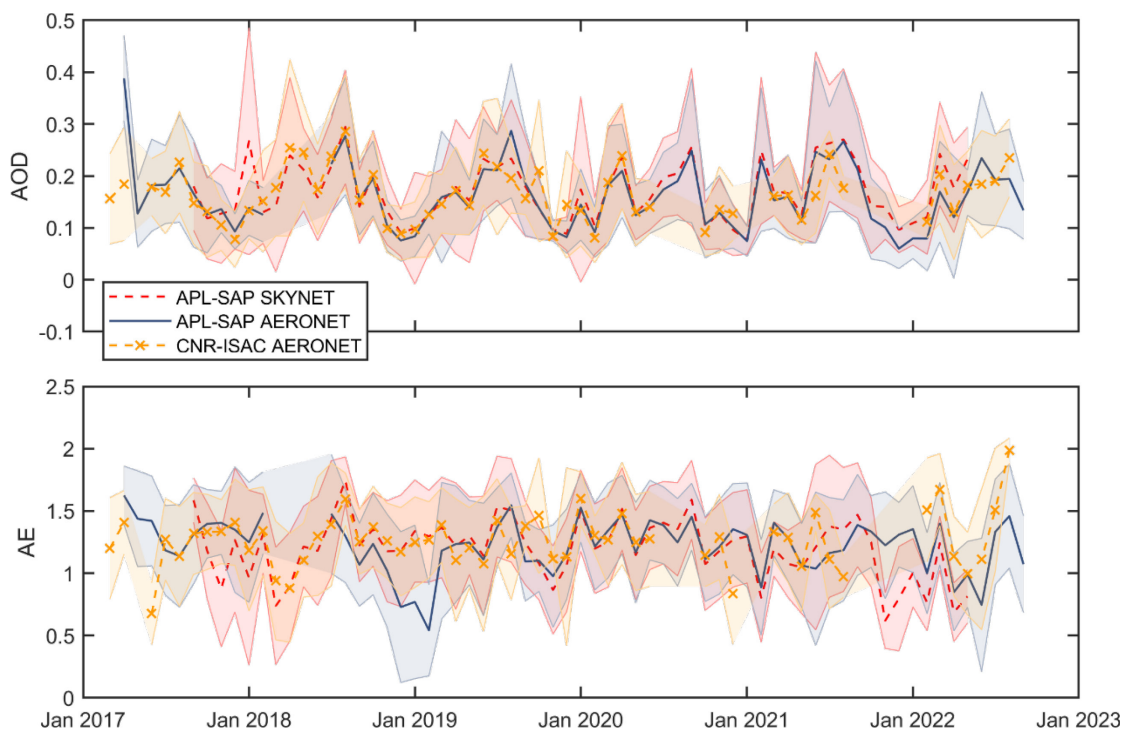
	TROPOMI NO ₂ Actual Measurements								TROPOMI NO ₂ Daily Mean								TROPOMI NO ₂ Monthly Mean								
	AERONET				SKYNET				AERONET				SKYNET				AERONET				SKYNET				
	CNR-ISAC	440	380	440	400	400	400	400	CNR-ISAC	440	380	440	400	400	400	400	400	CNR-ISAC	440	380	440	400	400	400	400
NO₂																									
Channel [nm]																									
% Mean Deviation	19.49	19.81	24.10	24.29	-	-	-	18.73	19.01	23.41	23.64	-	-	-	-	-	6.27	6.63	12.90	13.24	-	-	-	-	-
Mean Deviation [DU]	0.053	0.053	0.064	0.064	-	-	-	0.051	0.051	0.062	0.062	-	-	-	-	-	0.017	0.018	0.034	0.035	-	-	-	-	-
STD [DU]	0.048	0.048	0.066	0.067	-	-	-	0.046	0.046	0.064	0.064	-	-	-	-	-	0.019	0.018	0.025	0.025	-	-	-	-	-
Minimum Deviation [DU]	6×10 ⁻⁵	8×10 ⁻⁶	2×10 ⁻⁵	2×10 ⁻⁵	-	-	-	3×10 ⁻⁶	4×10 ⁻⁶	2×10 ⁻⁶	3×10 ⁻⁶	-	-	-	-	-	2×10 ⁻⁶	3×10 ⁻⁵	5×10 ⁻⁸	9×10 ⁻⁷	-	-	-	-	-
Maximum Deviation [DU]	0.408	0.422	0.565	0.567	-	-	-	0.398	0.412	0.564	0.566	-	-	-	-	-	0.103	0.089	0.149	0.151	-	-	-	-	-
NO_D																									
Channel [nm]																									
% Mean Deviation	0.536	0.574	0.855	0.845	3.784	3.784	0.517	0.550	0.839	0.814	0.814	3.812	3.812	3.812	3.812	3.812	0.169	0.182	0.538	0.451	3.865	3.865	3.865	3.865	3.865
Mean Deviation	0.0009	0.0008	0.0011	0.0009	0.0051	0.0051	0.0008	0.0007	0.0010	0.0009	0.0009	0.0051	0.0051	0.0051	0.0051	0.0051	0.0003	0.0003	0.0006	0.0005	0.0051	0.0051	0.0051	0.0051	0.0051
STD	0.0008	0.0007	0.0011	0.0010	0.0017	0.0017	0.0008	0.0007	0.0011	0.0009	0.0009	0.0017	0.0017	0.0017	0.0017	0.0017	0.0003	0.0003	0.0004	0.0004	0.0008	0.0008	0.0008	0.0008	0.0008
Minimum Deviation	1×10 ⁻⁶	1×10 ⁻⁷	3×10 ⁻⁷	4×10 ⁻⁷	0.0023	0.0023	5×10 ⁻⁸	6×10 ⁻⁸	4×10 ⁻⁸	5×10 ⁻⁸	5×10 ⁻⁸	0.0024	0.0024	0.0024	0.0024	0.0024	3×10 ⁻⁸	5×10 ⁻⁷	7×10 ⁻¹⁰	1×10 ⁻⁸	0.0038	0.0038	0.0038	0.0038	0.0038
Maximum Deviation	0.007	0.006	0.009	0.008	0.017	0.017	0.007	0.006	0.009	0.008	0.008	0.015	0.015	0.015	0.015	0.015	0.002	0.001	0.002	0.002	0.008	0.008	0.008	0.008	0.008
AE																									
Spectral Range [nm]	440-870	440-870	440-870	400-1020	400-1020	400-1020	440-870	440-870	440-870	440-870	440-870	400-1020	400-1020	400-1020	400-1020	400-1020	440-870	440-870	440-870	440-870	400-1020	400-1020	400-1020	400-1020	400-1020
% Mean Deviation	0.853	1.645	1.645	3.963	3.963	3.963	0.843	0.843	1.674	1.674	1.674	4.000	4.000	4.000	4.000	4.000	0.524	0.616	0.616	4.227	4.227	4.227	4.227	4.227	
Mean Deviation	0.009	0.012	0.012	0.038	0.038	0.038	0.009	0.009	0.011	0.011	0.011	0.038	0.038	0.038	0.038	0.038	0.006	0.005	0.005	0.039	0.039	0.039	0.039	0.039	
STD	0.011	0.017	0.017	0.026	0.026	0.026	0.010	0.010	0.016	0.016	0.016	0.027	0.027	0.027	0.027	0.027	0.004	0.006	0.006	0.027	0.027	0.027	0.027	0.027	
Minimum Deviation	1×10 ⁻⁷	1×10 ⁻⁷	1×10 ⁻⁷	0.001	0.001	0.001	2×10 ⁻⁷	2×10 ⁻⁷	7×10 ⁻⁸	7×10 ⁻⁸	7×10 ⁻⁸	0.001	0.001	0.001	0.001	0.001	1×10 ⁻⁷	7×10 ⁻⁸	7×10 ⁻⁸	0.002	0.002	0.002	0.002	0.002	
Maximum Deviation	0.116	0.239	0.239	0.286	0.286	0.286	0.116	0.116	0.238	0.238	0.238	0.393	0.393	0.393	0.393	0.393	0.036	0.090	0.090	0.252	0.252	0.252	0.252	0.252	



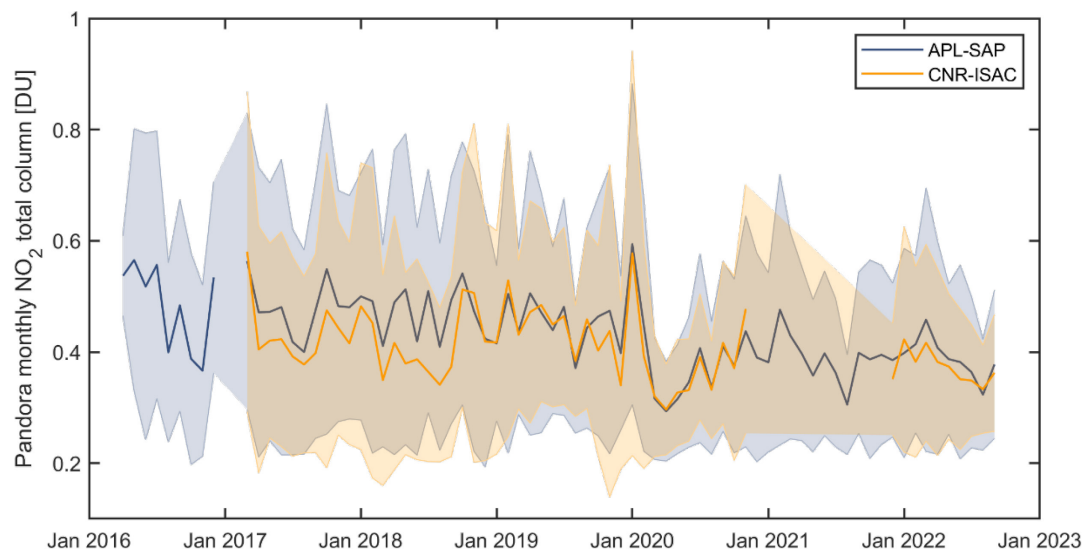
810 **Table 3.** AOD and AE trends and their uncertainties for both standard and modified AERONET and SKYNET products over CNR-ISAC and APL-SAP. Note that the spectral channels used in AERONET retrievals are 440 nm for AOD and 440-870 nm for AE, whereas for SKYNET are 400 nm and 400-1020 nm for AOD and AE, respectively. The trend uncertainties refer to the standard error of the regression slope. The differences are calculated on the absolute trend values.

		AERONET CNR-ISAC		AERONET APL-SAP		SKYNET APL-SAP	
		standard	modified	standard	modified	standard	modified
Number of years		5.7	5.7	5.7	5.7	5.4	5.4
AOD	Trend [/year]	0.0037	0.0024	0.00019	0.00052	0.0015	0.0018
	% trend [/year]	2.04	1.38	0.11	0.30	0.82	0.99
	Uncertainty	0.0054	0.0054	0.0049	0.0049	0.0062	0.0062
	Modified – standard		-0.0012 (-33.1%)		0.00033 (174.3%)		0.00024 (15.8%)
AE	Trend [/year]	0.0474	0.0416	-0.0221	-0.0181	-0.0611	-0.0569
	% trend [/year]	3.80	3.37	-1.85	-1.54	-5.56	-5.46
	Uncertainty	0.0252	0.0257	0.0184	0.0189	0.0256	0.0264
	Modified – standard		-0.0059 (-12.4%)		-0.0040 (-18.1%)		-0.0042 (-6.9%)

815



820 **Figure 1: Time series of monthly averaged AOD (upper panel) and AE (lower panel) measurements over APL-SAP (AERONET and SKYNET) and CNR-ISAC (AERONET). Note that AERONET AOD and AE correspond to the wavelength channels of 440nm and 440-870nm, respectively, whereas SKYNET AOD and AE refer to 400nm and 400-1020nm, respectively. The shaded areas correspond to the monthly 1-sigma deviation.**



825

Figure 2: Time series of monthly NO₂ total column from Pandora instruments over APL-SAP (blue line) and CNR-ISAC (yellow line). The shaded areas correspond to the 1-sigma standard deviation of the monthly averaged values. The NO₂ concentration is clearly affected by the COVID-19 lockdown during February – May 2020.



830

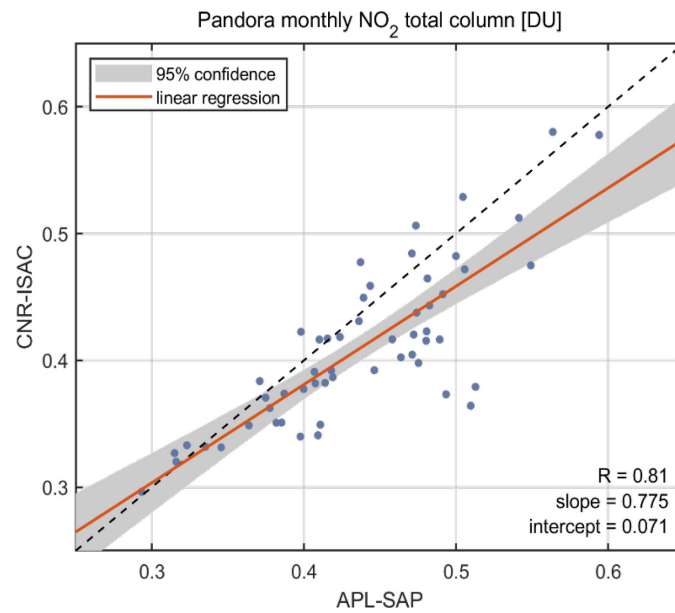
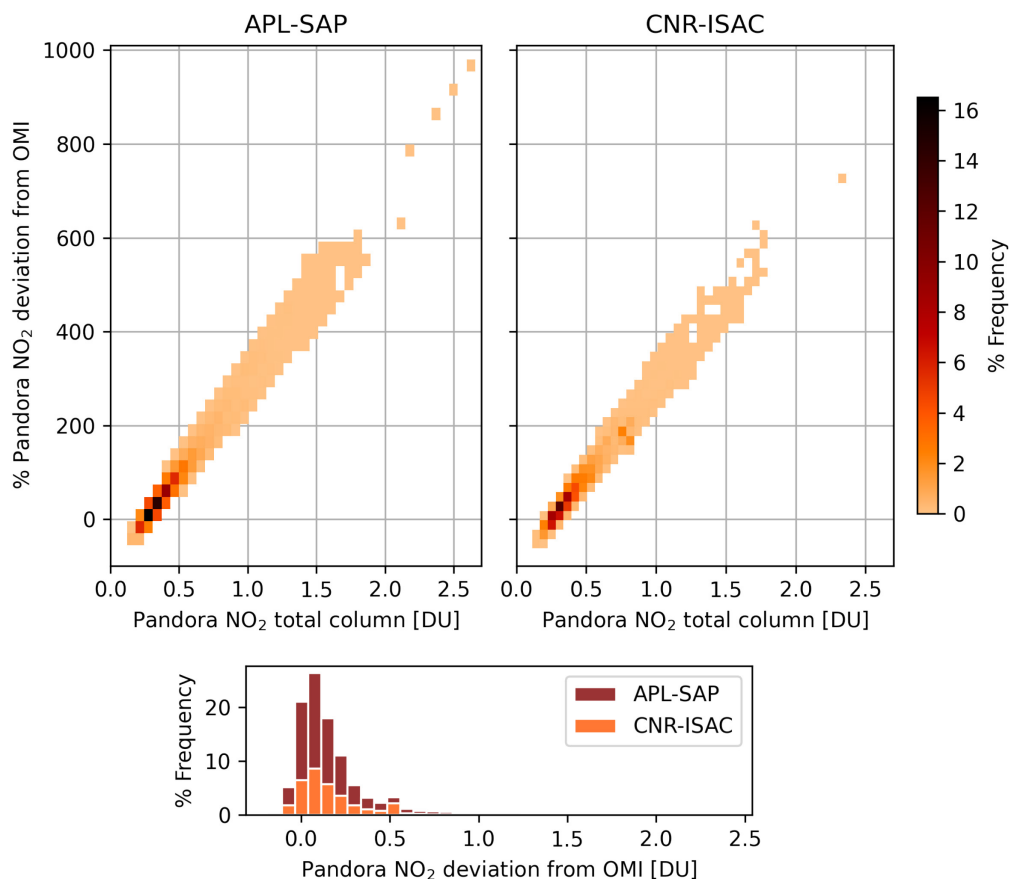


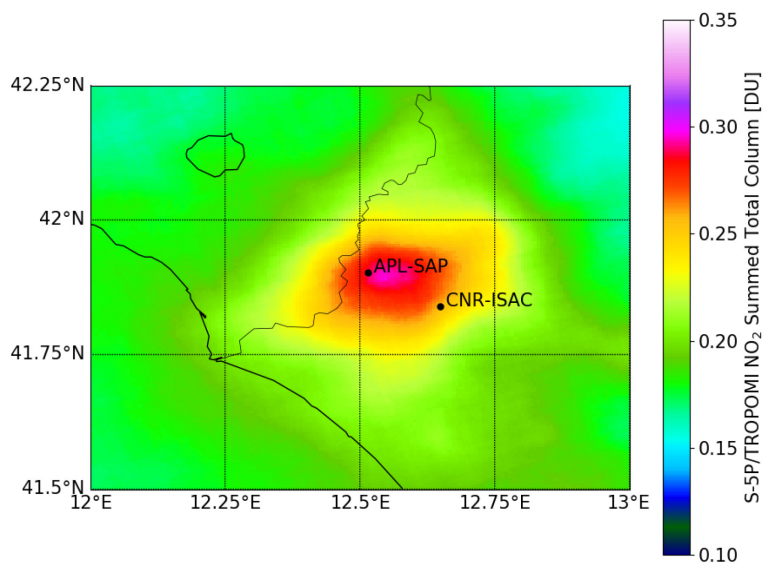
Figure 3: Monthly NO₂ total column from Pandora over CNR-ISAC against synchronous APL-SAP observations. The grey shaded area corresponds to the 95% confidence interval of the linear regression fit (red line).



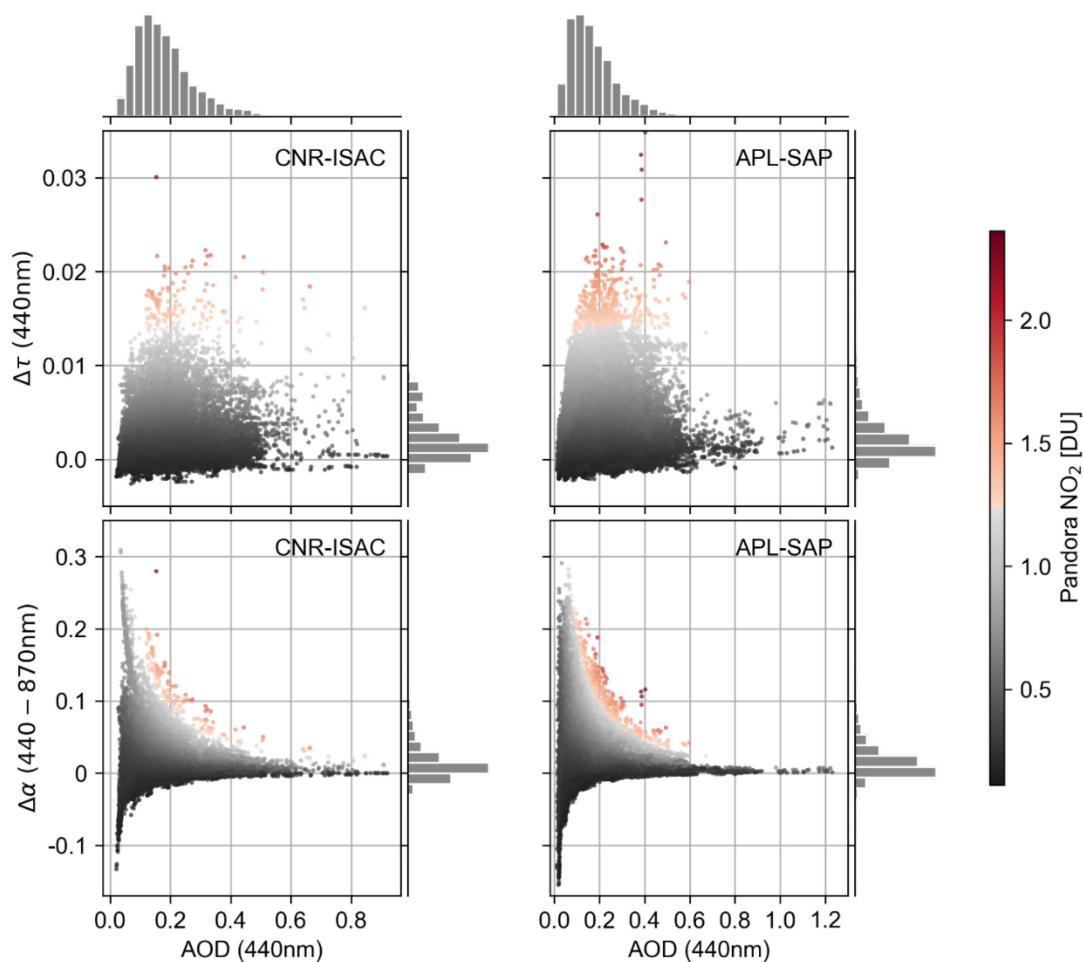
835



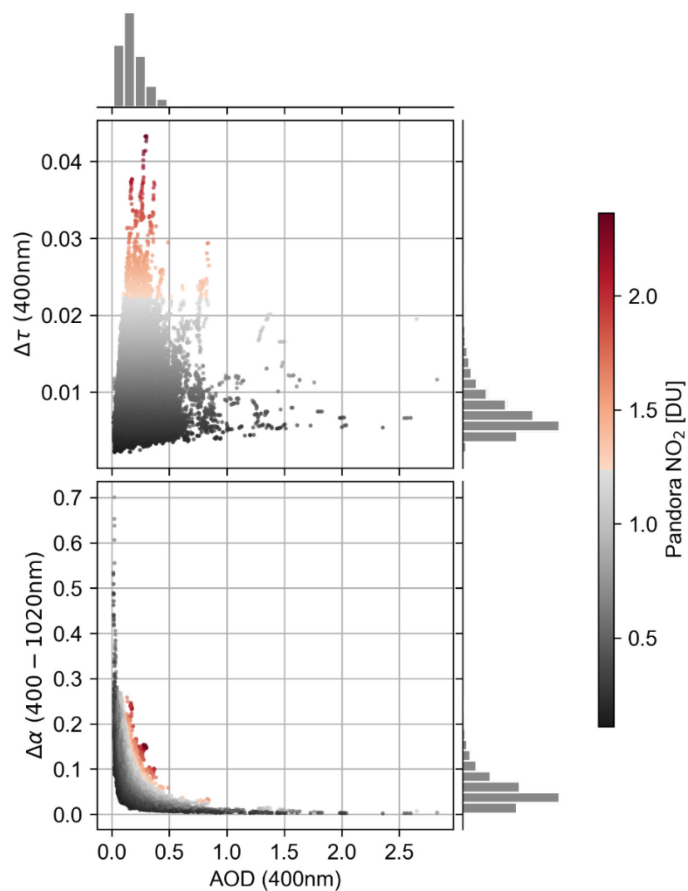
840 **Figure 4: Percentage deviation of Pandora total NO₂ data from AERONET NO₂ climatological values (OMI) for both APL-SAP (left upper panel) and CNR-ISAC (right upper panel) versus Pandora NO₂. The data pairs are grouped in color-scaled bins of bivariate percentage distribution. The relative frequency distributions of absolute Pandora-OMI deviation for both locations are illustrated in the lower panel. Note that the distribution bars for the two locations are stacked.**



845 **Figure 5: S5P/TROPOMI summed total NO₂ column averaged for the period 2018-2021, excluding the COVID-19 lockdown period. The data are gridded on a 500m grid. The locations of the two observational sites used in this study are also reported for reference.**

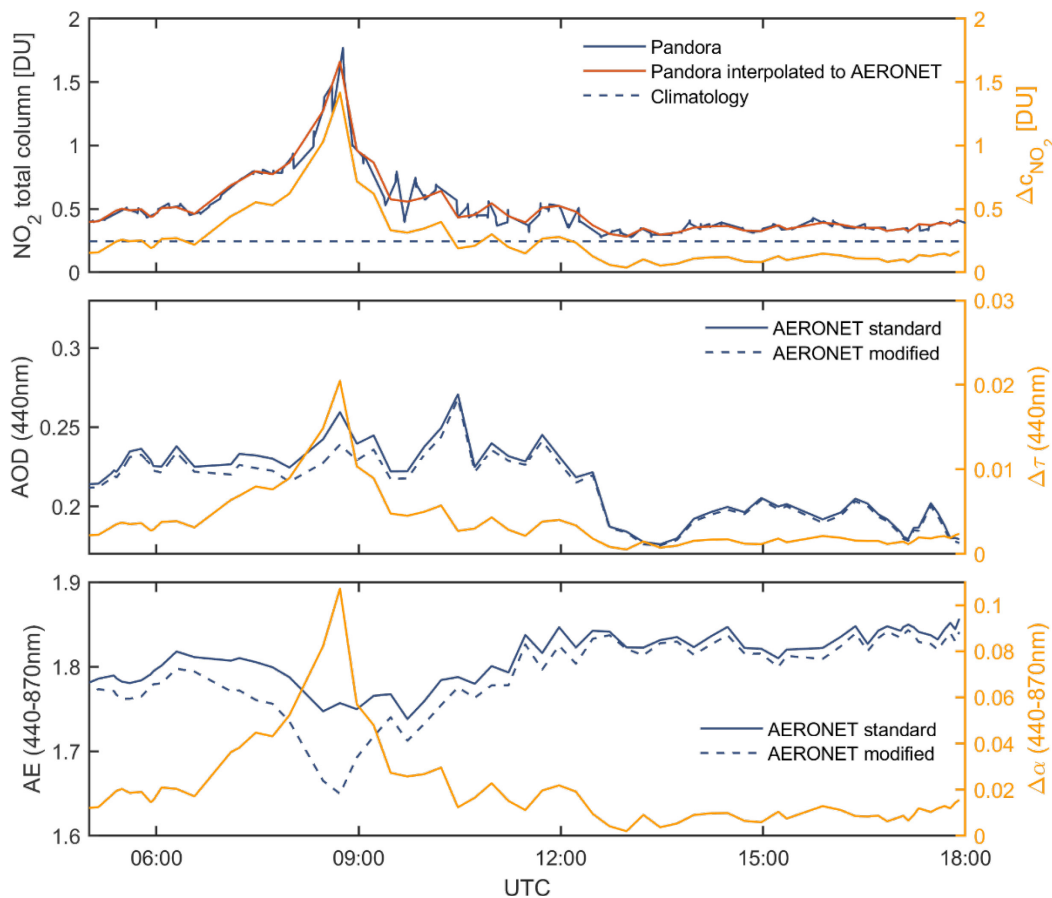


850 **Figure 6:** The differences of modified AERONET AOD at 440 nm (upper panels) and AE at 440-870 nm (lower panels) over CNR-ISAC (left panels) and APL-SAP (right panels) from the standard products illustrated with respect to the standard AERONET AOD measurements at 440 nm and the actual NO₂ observed by Pandora (color scale). The corresponding distributions of all variables are also included.



855

Figure 7: Similar to Fig. 6, but for SKYNET retrievals over APL-SAP. Note that the spectral channels for the retrievals are different compared to AERONET, i.e. 400nm for AOD and 400-1020nm for AE. Also the axis scales are different.



860

Figure 8: Case study over APL-SAP for 25th June 2020. Upper panel: Pandora total NO₂ column and its deviation from climatology. Middle panel: AERONET AOD (solid blue line), its improvement using Pandora NO₂ (dashed blue line) and the magnitude of improvement (light orange line and right y-axis). Lower panel: Similar to middle panel, but for AE retrievals.



865

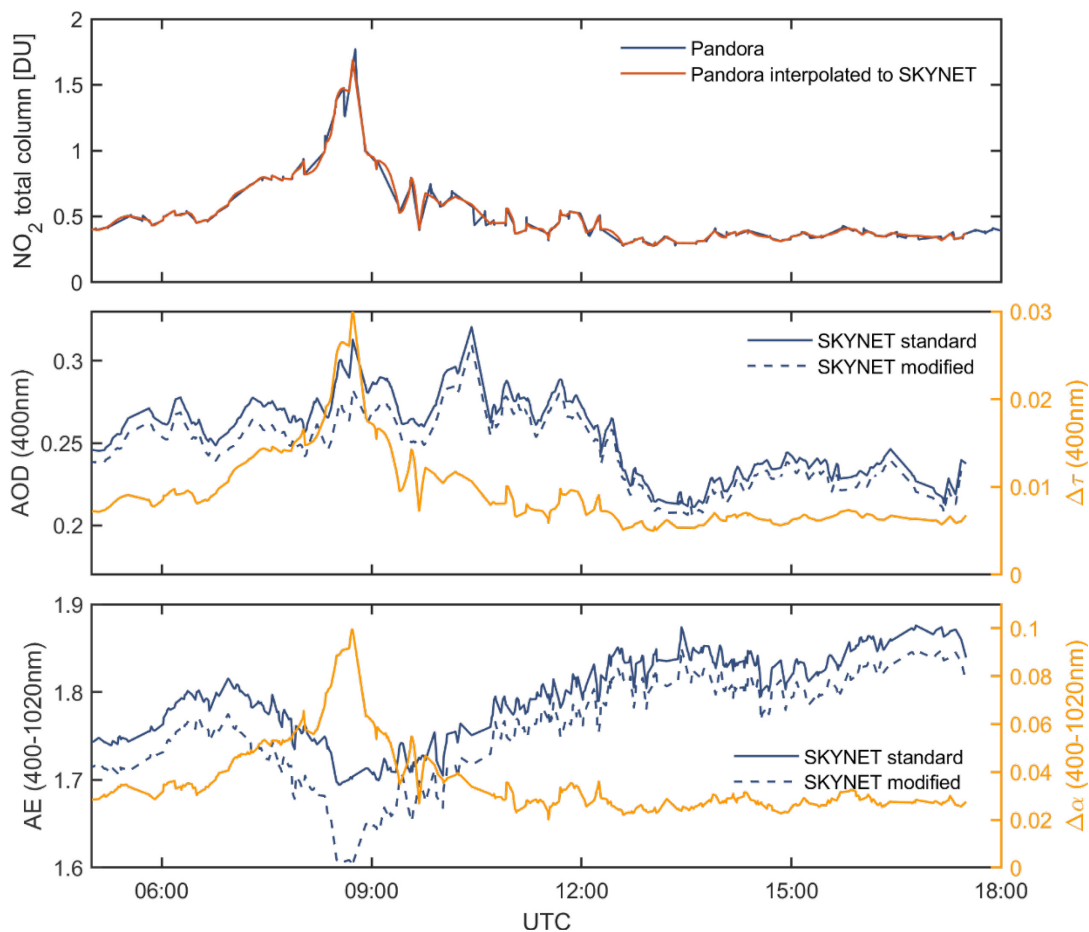


Figure 9: Similar to Fig. 8, but for SKYNET retrievals over APL-SAP location. Note that the spectral channels for the retrievals are different compared to AERONET.



870

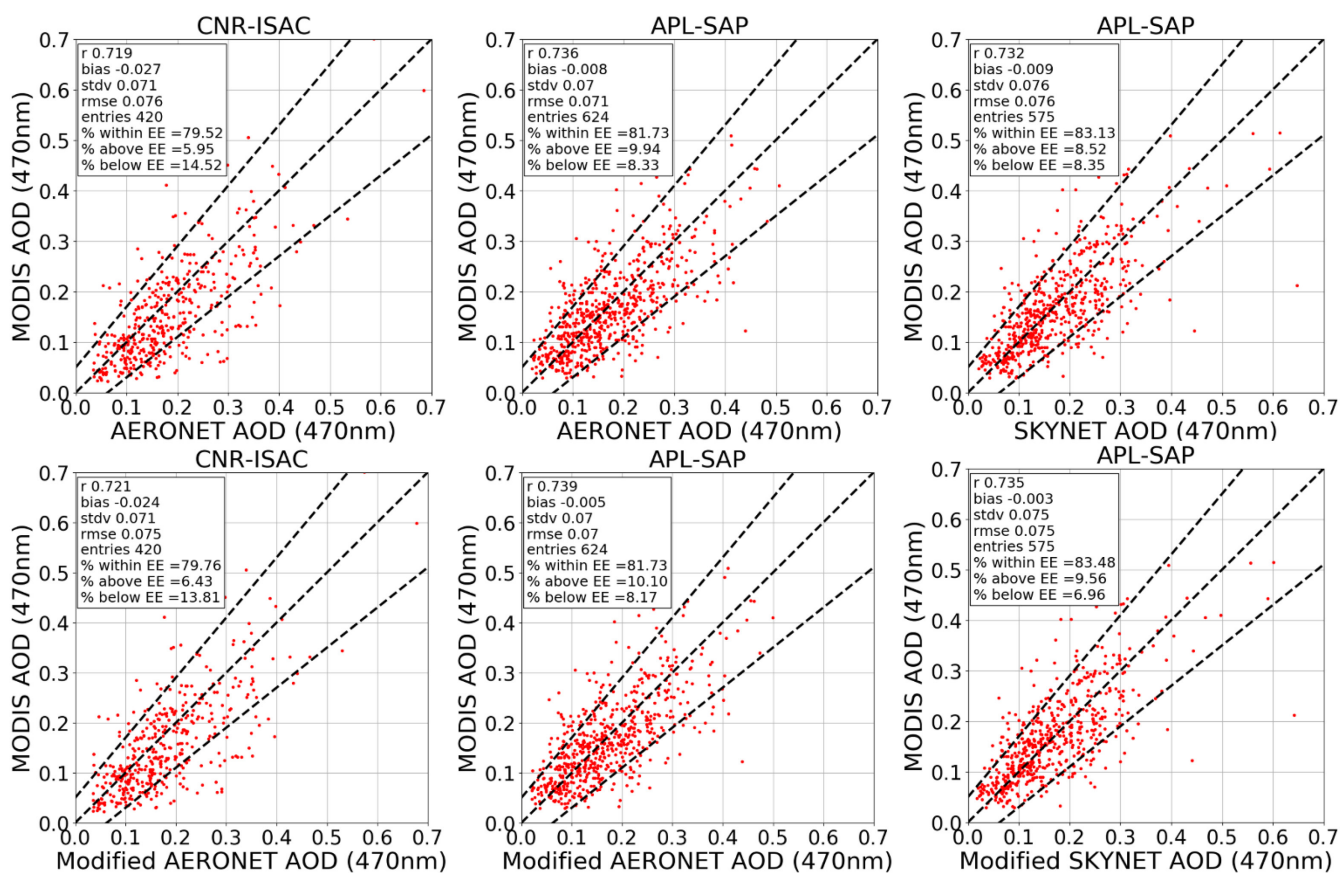
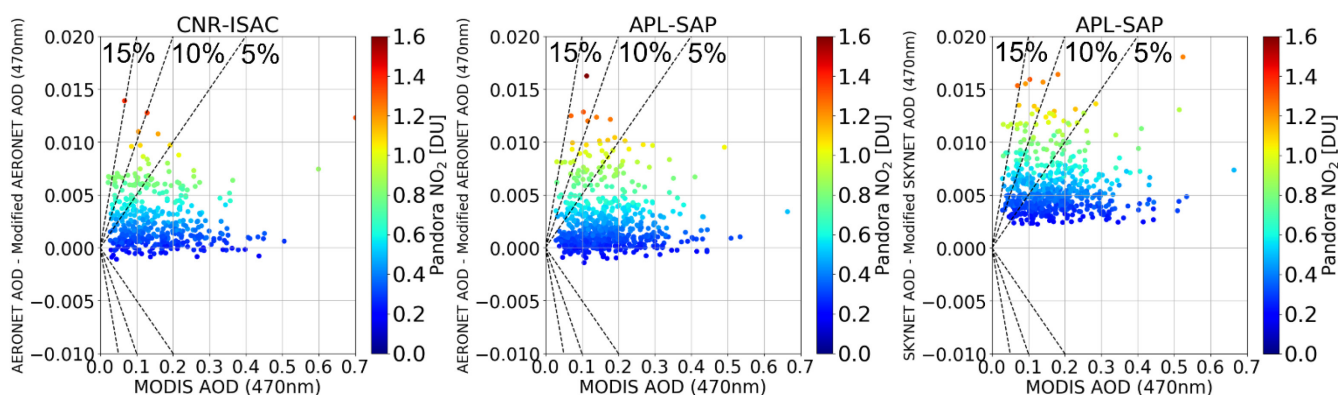


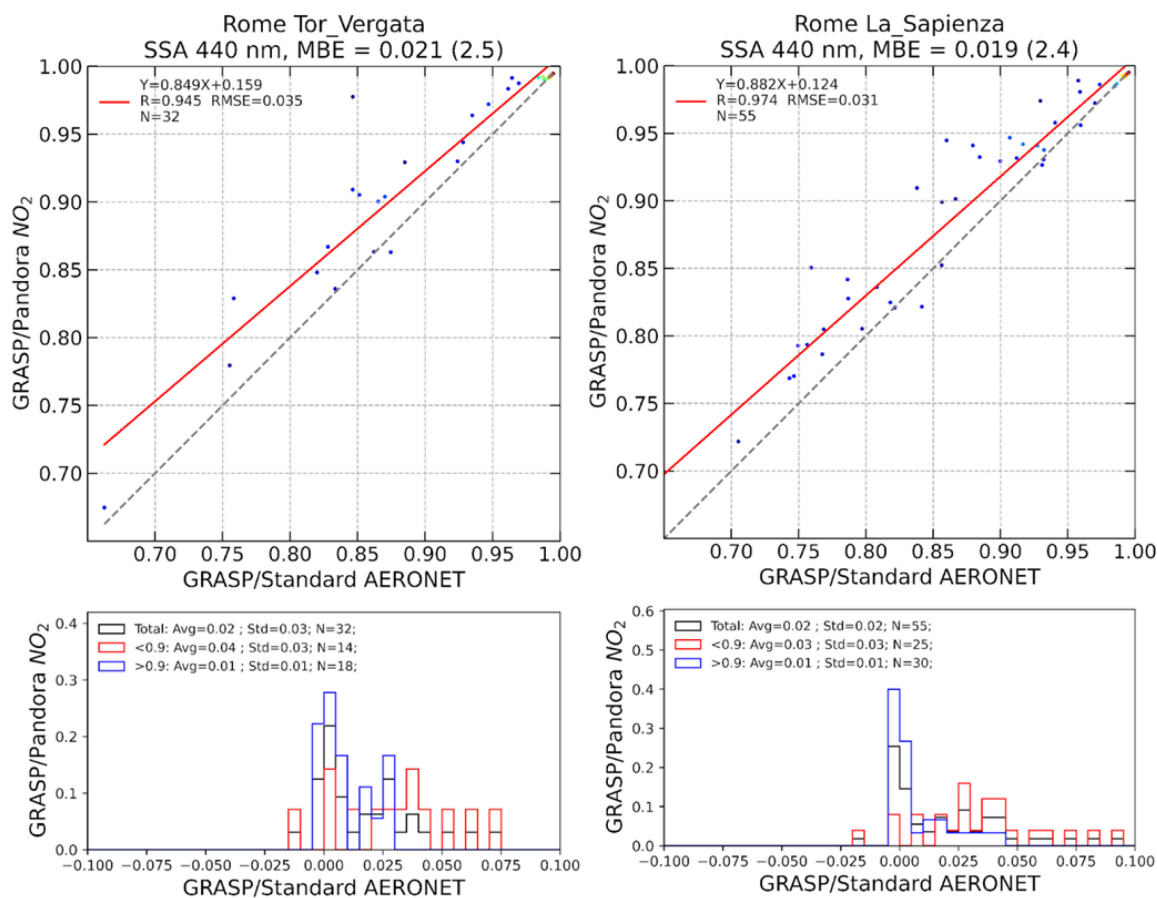
Figure 10: Inter-comparison of MODIS DB with standard (upper panels) and modified (lower panels) ground-based AOD at 470 nm for CNR- ISAC (left panels) and APL-SAP (middle and right panels) sites. In the left and middle panels, against AERONET AOD products, whereas in the right panels against SKYNET AOD. The $y=x$ lines and MODIS DB EE envelopes $\pm(0.05 + 20\%)$ are plotted as dashed lines. The inter-comparison was performed considering a maximum distance between the center of the MODIS DB pixel and the site location of 5 km and Δt_{\max} (time between MODIS and AERONET/SKYNET observations) of ± 30 minutes.

875



880 **Figure 11: Absolute correction as a function of the corresponding MODIS DB AOD data and PGN NO₂ data for CNR-ISAC (left panel) and APL-SAP (middle and right panels) sites. In the left and middle panels the inter-comparison was performed using AERONET AOD products, in the right panel SKYNET AOD were used. The color scale represents the PGN NO₂ retrieved in correspondence of the AERONET/SKYNET AOD products. The analysis was performed considering a maximum distance between the center of the MODIS DB pixel and the site location of 5 km and Δt_{max} of ± 30 minutes.**

885



890 **Figure 12:** Comparisons of SSA at 440 nm obtained with GRASP following the standard AERONET procedure (X axis) and a similar approach but precisely accounting for NO₂ concentration (Y axis) from the co-located Pandora instruments in two different stations: APL-SAP (right panel) from March 2017 to November 2020, and CNR-ISAC (left panel) from April 2017 to September 2021. The data has been filtered to show retrievals corresponding to NO₂ concentration higher than 0.9 DU. The absolute Mean Bias Error (MBE) (percent in parenthesis), the Root Mean Square Error (RMSE) and the correlation coefficient of the linear fit are also shown in the figures.